

Copyright
by
Ramakrishnan Kannappan
2009

**The Dissertation Committee for Ramakrishnan Kannappan Certifies that this is the
approved version of the following dissertation:**

**Design and Analysis of an Electronically Switchable Ion Exchange
System**

Committee:

Lynn E. Katz, Co-Supervisor

James A. Holcombe, Co-Supervisor

Gerald E. Speitel Jr.

Desmond F. Lawler

Howard M. Liljestrand

**Design and Analysis of an Electronically Switchable Ion Exchange
System**

by

Ramakrishnan Kannappan B.S.; M.S.

Dissertation

Presented to the Faculty of the Graduate School of

The University of Texas at Austin

in Partial Fulfillment

of the Requirements

for the Degree of

Doctor of Philosophy

The University of Texas at Austin

December 2009

Dedication

To my parents for always encouraging me, to my siblings for teaching me so many things through the years and making me who I am today, and to my wife for her love and support.

Acknowledgements

I would like to thank Dr. Lynn Katz for everything she has done to change my life since I met her 8 years ago. I have changed fields, learned so many new things about science and about myself, and become a better engineer and scientist thanks to her. I could not have completed my work without her guidance and support. I would also like to thank Dr. James Holcombe for his support and enthusiasm throughout my time working with him. I worked in his lab and his insight and advice was always appreciated. Also I want to thank Dr. Chia-chen Chen for taking me out to Stanford and carrying me through the EXAFS portion of my work.

Thanks to all the graduate students that I worked with over my time at Texas, especially the Katz and Holcombe research groups. They taught me how to work in the lab, provided countless hours of distractions when needed, and always encouraged each other. I would also like to thank the graduate students on the 9th floor who preceded me for making my graduate school experience that much better.

Thanks to my friends from high school and all my friends in Austin who still support me to this day, even at my dissertation defense. I want to thank my parents for all the little things they did over the years to support me, and my siblings for being hard on me at times and teaching me all the time. Finally, I would like to thank my wife for her caring encouragement over the past year and the years to come.

Design and Analysis of an Electronically Switchable Ion Exchange System

Publication No. _____

Ramakrishnan Kannappan

The University of Texas at Austin, 2009

Co-supervisors: Lynn E. Katz, James A. Holcombe

Metal contamination is a considerable environmental problem because metals are persistent contaminants. Ion exchange is one of the most commonly used treatment options for trace metal removal. This research develops and evaluates a redox active modified ion exchange system that has the potential to reduce the ionic strength of ion exchange regeneration streams. Poly-L-cysteine (PLC) was selected as the redox active, adsorbing functional group on the surface of a reticulated vitreous carbon (RVC) electrode. PLC is an excellent soft acid metal chelator and is unique in that its thiol groups can form disulfide bonds with each other. The reduction of available thiols changes the metal binding capacity of the peptide since the thiol is the primary binding group. RVC provides a macroporous conductive monolithic resin to support the peptide. An experimental apparatus was designed to study the properties of this system and estimate performance.

Distinct oxidized and reduced states of PLC on the surface of the RVC were confirmed by changes in metal binding characteristics. Adsorption edges showed a sharper pH dependence for the reduced electrode compared to the oxidized electrode from pH 3-7. Adsorption isotherms performed at pH 7 showed increased capacity for the reduced electrode. The change was reversible by chemical and electrical reduction. This difference was confirmed at the molecular level with Cd- EXAFS of oxidized and reduced electrodes. A greater degree of cadmium-sulfur coordination was observed on the reduced electrode and a greater cadmium-oxygen coordination was apparant on an oxidized electrode. A multidentate adsorption model was developed to model the pH dependent behavior of cadmium adsorption on the PLC-RVC surface. Nickel adsorption showed increased adsorption in the oxidized state. The most likely explanation is increased carboxylate complexation.

The electronically switchable ion exchange system (ESIE) provides a framework for modifying traditional ion exchange processes. The system has 5 to 10 times less specfic capacity than current ion exchange systems, but uses solutions 10-100 times lower in ionic strength for regeneration. Further studies on the effect of ionic strength on adsorption and current usage are necessary to compare the cost of the ESIE process to traditional ion exchange.

Table of Contents

List of Tables	x
List of Figures	xi
Chapter 1: Introduction	1
1.1 Problem Statement	1
1.2 Present State of Knowledge	1
1.3 Objectives and Hypotheses	3
1.4 Research Overview	4
1.5 Thesis Structure	4
Chapter 2: Literature Review	6
2.1 Metals Removal Technologies	6
2.2 Modifications to Ion Exchange	9
2.2.1 Electrochemically Switched Ion Exchange systems	12
2.3 Metal Binding Peptides	13
2.3.1 Polypeptides	13
2.3.2 Structure and binding of polypeptides	16
Chapter 3: Design and analysis of a bench scale ESIE apparatus	19
3.1 General Design requirements for a bench scale ESIE system	19
3.2 Experimental Methods	19
3.2.1 Instrumentation	19
3.2.2 Reagents	20
3.2.3 System Construction and Assembly	20
3.2 Substrate Preparation	22
3.2.1 Substrate material selection	22
3.1.1 Peptide attachment	26
3.3 System Design and Layout	28
3.3.1 System Requirements	28
3.3.2 System Design	29

3.4 Electrochemical Characteristics	36
Chapter 4: Metal adsorption on the ESIE apparatus	39
4.1 Methods.....	39
4.1.1 Instrumentation	39
4.1.2 Reagents	40
4.1.3 Rate Analysis	40
4.1.4 Adsorption Edges and Isotherms	41
4.1.5 XAS Procedure	43
4.1.6 XAS Data Analysis	45
4.2 Estimation of Time to Apparent equilibrium.....	46
4.3 Cadmium Adsorption results	48
4.3.1 pH dependent adsorption behavior of Cd^{2+}	48
4.3.2 Cadmium Adsorption Isotherm Results.....	50
4.3.3 Cadmium PLC-RVC XAS Analysis and Results	56
4.4 Cadmium Adsorption Model Development.....	64
4.4.1 Baseline Model	64
4.4.2 Multidentate model for Cd^{2+} sorption.....	70
4.5 Nickel Adsorption Results	77
4.5.1 pH dependent adsorption behavior of Ni^{2+}	77
4.5.2 Ni Adsorption Isotherm results	79
4.6 Summary	81
Chapter 5: Conclusions and Recommendations	83
5.1 Engineering Implications	85
5.2 Recommendations.....	87
Appendix – Model Calculations	88
Glossary	89
References	90
Vita	95

List of Tables

Table 1. Maximum Contaminant Levels and Potential Health Effect for Selected Heavy Metals	7
Table 2. Common categories of functional groups found on ion exchange resins	9
Table 3. Approximate relative selectivity values for a strong acid ion exchange resin ...	11
Table 4. Substrate Material Options	24
Table 5. Physical properties of 900 ppi Reticulated Vitreous Carbon	25
Table 6. Redox potentials of reagents	53
Table 7. Estimated Cadmium Capacity for PLC-RVC Isotherm Experiments	55
Table 8. EXAFS Parameters	61
Table 9. Best fit parameters for the baseline model.....	68
Table 10. Multidentate model parameters	72
Table 11. Best fit parameters for the multidentate model.....	73
Table 12. log K values for complexation of Ni and Cd with two representative amino acids	79

List of Figures

Figure 1. Metal binding scheme.....	2
Figure 3. Chemical structure of cysteine and poly-L-cysteine (PLC)	15
Figure 4. Breakthrough curves for Cd^{2+} at pH 7 on a PLC functionalized controlled pore glass column.....	17
Figure 4. Cyclic Voltammogram of a cysteine functionalized activated carbon cloth in 1 M H_2SO_4 . Carbon mass = 10 mg, Scan Rate = 1 mV/s	24
Figure 5. Examples of Reticulated Glassy Carbon foams from ERG Aerospace.....	25
Figure 6. MALDI analysis of synthesized PLC peptide.	27
Figure 7. Peptide immobilization reaction.....	28
Figure 8. Top and Front views of the electrode housing	31
Figure 9. Side and wireframe isometric views of the electrode housing	32
Figure 10. Top and front views of the inlet.	33
Figure 11. Side and wireframe isometric views of the inlet	34
Figure 12. Primary components of the lab scale ESIE system	35
Figure 13. ESIE System Schematic	36
Figure 14. Current usage for electrochemical reduction (a) and oxidation (b) of RVC- PLC at -0.8 V and +0.8 V vs Ag/AgCl with 0.05, 0.2 and 1 M KCl.....	37
Figure 15. Nickel concentration in a batch kinetic test of adsorption onto a PLC electrode	47
Figure 16. Cadmium concentration in a batch kinetic test of adsorption onto Gly, Cys, and PLC electrodes.	47

Figure 17. Cadmium adsorption/desorption edge on reduced (a) and oxidized (b) PLC-RVC (10 mg/L total metal concentration, 0.015 M ionic strength).....	49
Figure 18. Cd^{2+} adsorption density onto DTT reduced and two H_2O_2 oxidized PLC-RVC electrodes. Normal scale (a) and log-log scale (b).....	51
Figure 19. Cd^{2+} adsorption density onto DTT and electrochemically reduced PLC-RVC electrodes. Several redox cycles were performed between the two trials. Normal scale (a) and log-log scale (b).	52
Figure 20. Cd^{2+} adsorption density onto a NaBH_4 modified PLC-RVC electrode. Initial reduction and electrochemical and H_2O_2 oxidations are compared. Normal scale (a) and log-log scale (b).....	54
Figure 21. XANES Spectra for Cd^{2+} on reduced and oxidized PLC-RVC.	58
Figure 22. (a) EXAFS Spectra of Cd^{2+} on reduced PLC-RVC and (b) Fourier Transformed EXAFS Spectra of Cd^{2+} on reduced PLC-RVC.....	59
Figure 23. (a) EXAFS Spectra of Cd^{2+} on oxidized PLC-RVC and (b) Fourier Transformed EXAFS Spectra of Cd^{2+} on oxidized PLC-RVC. Dashed lines are data and solid lines represent the components of the fit and the total fit.	60
Figure 24. Coordination numbers of Cd-O (a) and Cd-S (b) bonds	63
Figure 25. Breakthrough curves for Cd^{2+} adsorbing to reduced PLC immobilized on controlled pore glass. Influent concentration = 10 mg/L Cd^{2+}	64
Figure 26. pH dependent site-limited model prediction of metal adsorption ($\text{Me}_{\text{TOT}} = 1 \times 10^{-4}$ M, $\text{S}_{\text{TOT}} = 2 \times 10^{-4}$ M, $K = 0.05$, $K_a = 1 \times 10^{-10}$ M)	67
Figure 27. Baseline model fit for Cd^{2+} on reduced PLC-RVC. $K = 1.5$, $\text{S}_{\text{tot}} = 9.8 \times 10^{-5}$ M	68

Figure 28. Baseline model fit for Cd^{2+} on oxidized PLC-RVC. $K = 0.49$, $S_{\text{tot}} = 5.4 \times 10^{-5} \text{ M}$	69
Figure 29. Multidentate model fits for Cd^{2+} on reduced PLC-RVC as percent adsorbed (a) and log Cd^{2+} concentration (b).....	74
Figure 30. Multidentate model fits for Cd^{2+} on oxidized PLC-RVC RVC as percent adsorbed (a) and log Cd^{2+} concentration (b).....	75
Figure 31. Ni^{2+} adsorption edge on DTT reduced and H_2O_2 oxidized PLC-RVC.	78
Figure 32. Ni^{2+} adsorption onto DTT reduced and H_2O_2 oxidized PLC-RVC electrodes. Normal scale (a) and log-log scale (b).....	80

Chapter 1: Introduction

1.1 PROBLEM STATEMENT

Metal contamination is a considerable environmental problem because metals are a persistent contaminant. Metals cannot be degraded like organic contaminants so they tend to accumulate over time [1]. Sources of contamination range from release of naturally occurring metals such as arsenic in groundwater to anthropogenic sources such as mercury in runoff from mining operations. Many of these metals have health effects at trace concentrations and present a treatment challenge. Maximum contaminant levels (MCLs) for drinking water have been set at concentrations as low as 10 µg/L for arsenic and cadmium. Many conventional treatment options such as precipitation cannot reduce contaminant concentrations to these levels without additional treatment. To achieve low levels, polishing steps such as ion exchange or electrodeposition are required. The products of these processes are contaminated sludges and brines that present a significant treatment challenge themselves. Existing treatment options move metals from one waste stream to another, but do not provide a sustainable endpoint for the waste. A process that produces a waste stream which itself is not difficult to treat provides a more sustainable end point for metal containing wastes. A reduction in chemicals used to regenerate a system improves the nature of the waste created.

1.2 PRESENT STATE OF KNOWLEDGE

A possible solution to the remediation and waste processing problem is to add electrochemical modification to ion exchange. Redox chemistry can be used to affect the surface chemistry of an electrically conductive resin. A potential applied to the surface of a conductive resin can change conformation or chemical structure of an electroactive

molecule bound to that surface. Since a change in chemistry can affect metal binding affinity, a mechanism to ‘switch’ the binding affinity of a resin is created by this change in surface chemistry. A suitable molecule could provide both binding capacity and redox activity to affect the binding affinity. One set of molecules that fit these requirements are metalloproteins, which have shown a strong binding affinity for a variety of metals [2]. The metal binding affinity and redox activity of the metalloproteins are defined by the amino acid composition of the protein. An amino acid residue with reversible electrochemistry is cysteine, which contains an electrochemically active thiol group. For example, two adjacent thiol groups form a disulfide bond under oxidizing conditions, which can be reduced back to free cysteines. The disulfide-bonded cysteine has a much lower metal binding affinity than free cysteine [3, 4]. Poly-L-Cysteine (PLC) is a synthetic homopolymer which consists of only cysteine residues. Oxidized PLC forms disulfide bonds with itself and neighboring PLC molecules. The overall binding capacity is reduced by decreasing the number of free cysteine residues and also by the formation of a tight secondary structure as shown in Figure 1. This bind and release mechanism has been supported by atomic force microscopy [5].

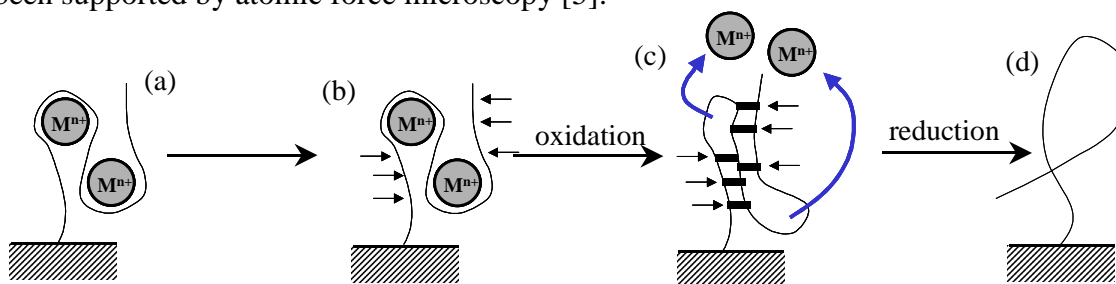


Figure 1. Metal binding scheme. (a) Cations bind to free sulfhydryl groups on the amino acid chain. (b) An oxidative potential is applied to the surface. (c) Disulfide bonds are formed in the oxidative environment, and the binding affinity for the metal drops. The metal is then released and can be rinsed away. (d) The amino chain is reduced to restore the original metal binding affinity.

A contaminated stream can be remediated by binding a specific metal onto the resin, and then the metal can be released into a concentrated, smaller volume of fluid.

The waste stream from this process will have a lower salt concentration than regeneration brines produced from ion exchange. Also, the process uses less power than electrodeposition processes, because only the surface amino acids are oxidized and reduced, not the metal ions themselves. If the metals are directly reduced, the current requirement becomes significant since 96,485 coulombs of charge are needed per equivalent of metal reduced from Faraday's constant. With this electronically switchable ion exchange (ESIE) system, the current required is a function of the surface area of the resin, the density of protein on the surface and the number of metals ions bound per protein. The combination of cleaner waste product and a reduction in power usage can reduce the overall cost of treating wastes containing metals while still maintaining a similar level of sustainability.

1.3 OBJECTIVES AND HYPOTHESES

Preliminary research suggests that this technology could be viable; however, many research questions remain as we translate our understanding of the chemistry of this process to engineered systems. Johnson and Holcombe have shown binding and release through ESIE at a nanogram per cm^2 level for several soft acid metals [6]. However they used a low surface area carbon disk electrode which severely limited their capacity. A viable wastewater treatment process requires a removal capacity several orders of magnitude greater. This research attempts to examine the issues associated with scaling an electrochemical process while continuing to explore the fundamentals associated with the ESIE process.

The following hypotheses were tested in this research:

- I. Distinct oxidized and reduced states of the PLC-RVC electrode could be produced

- II. The two oxidation states of the electrode have different metal ion adsorption properties
- III. The oxidation states of the electrode can be switched by application of a potential.

1.4 RESEARCH OVERVIEW

To test these hypotheses, this research was broken into two phases. First an apparatus was designed to perform redox chemistry on a high surface area conductor with polypeptides attached. This involved selection of a substrate material, choice of a method to attach a peptide to the surface, and creation of an electrode from the substrate. The electrode was then placed in a structure to allow simultaneous equilibrium measurement and application of potential. The nature of the peptide on the surface was then assessed by chemical means. Differences in chemical properties of the surface under oxidized versus reduced conditions were used to evaluate the first hypothesis. Second, the metal binding capacity of the electrode was evaluated. The surface of the electrode was reduced and oxidized by chemical and electrochemical means. Adsorption edges and isotherms were measured using cadmium and nickel as probes of the surface reactivity. Surface analysis of the electrodes with cadmium was undertaken by XPS and EXAFS. Changes in binding affinity and surface interaction were used to test the second and third hypotheses.

1.5 THESIS STRUCTURE

Chapter 2 provides a review of the literature relevant to ESIE. Chapter 3 details the design and fabrication of a system to evaluate the characteristics of metal binding in the ESIE system. Chapter 4 covers metal adsorption and spectroscopic experiments. In addition a model for metal adsorption within the system is developed. Chapter 5 states

conclusions on the hypotheses drawn and discusses future areas of investigation for the ESIE system.

Chapter 2: Literature Review

The electronically switchable ion exchange (ESIE) system that was developed in this research was predicated on the integration of metal ion adsorption and ion exchange properties, redox behavior of sulfur containing compounds, and electrochemistry of carbonaceous materials. In this chapter, literature in these areas that is relevant to ESIE design and operation is presented. Current metals removal technologies were evaluated and the relative advantages of ESIE were explored. Previous work was reviewed in the areas which make ESIE unique – use of metal binding peptides and the use of potential to affect binding. Information in these areas provided the design basis for the ESIE system.

2.1 METALS REMOVAL TECHNOLOGIES

Metals are a persistent problem in the environment even at relatively low concentrations. Current drinking water maximum contaminant levels and health effects for selected heavy metals are presented in Table 1. Often secondary treatment is necessary to reduce contaminant concentrations to levels that do not present health concerns. Several technologies exist that can achieve required effluent standards but each has drawbacks. The most widely used technologies for metal removal in aqueous solution are based on ion exchange. A difference in selectivity for two different ions is exploited when an innocuous ion bound to the surface of a resin is displaced by a contaminant ion. The resin is regenerated by overcoming the selectivity difference with a high concentration of the innocuous ion. The surface of the resin either has intrinsic metal binding properties or is functionalized with a chemical group that shows preference for a certain family of ions over others. The choice of group determines the nature of the resin. Negative groups such as carboxylates (COOH^-) give cation exchange resins and

quaternary amine groups (R_3N^+) give anion change resins. The resin itself is often a polymer which is resistant to the waste and regeneration streams [8]. Ion exchange resins range in capacity from 0.1 milliequivalents per gram (meq/g) for zeolites to 10 meq/g for synthetic resins [9].

Table 1. Maximum Contaminant Levels and Potential Health Effect for Selected Heavy Metals [7]

Metal	MCL (mg/L)	Potential Health Effects from Ingestion of Water
Arsenic	0.01	Skin damage or problems with circulatory systems
Cadmium	0.005	Kidney Damage
Chromium (total)	0.1	Allergic Dermatitis
Lead	0.015	Delays in physical or mental development; Kidney problems; high blood pressure
Mercury (inorganic)	0.002	Kidney Damage
Selenium	0.05	Hair or fingernail loss; numbness in fingers or toes; circulatory problems

Electrocoagulation uses principles similar to conventional coagulation to lower metal concentrations by trading chemical usage for electricity costs and system complexity [10]. A sacrificial anode (Fe or Al) is oxidized to release metal ions in solution in a manner similar to iron or alum addition. These ions precipitate and subsequently enmesh other particles and occlude contaminants in a manner similar to conventional coagulation. pH is increased by the reduction of protons to H_2 at the cathode. Less chemical pH adjustment is required, which lowers the cost of treatment relative to conventional treatment. The technology is currently maturing and has not been adopted on a large scale [10]. Several membrane based processes are often used for

ion removal such as reverse osmosis or electrodialysis. Reverse osmosis has the ability to separate metal contaminants, but generally requires a high quality feed stream to prevent membrane fouling [9]. Colloidal particles, bacterial activity, and scaling as a result of precipitation contribute to degradation of membrane flux. These problems limit the range of waters that are efficiently treated by reverse osmosis without pretreatment. Electrodialysis uses ion selective membranes to concentrate ions into specific channels of the apparatus, which reduces the contaminant concentration in the remaining cells. Electrodialysis can handle much higher dissolved solute concentrations than reverse osmosis, but still has similar fouling problems. In addition each equivalent of ions moved from the diluate to concentrate stream necessitates 96,485 coulombs (one Faraday) of charge to be passed through the apparatus. Since the system is built from a stack of channels, resistance through the membranes and solution is additive. Significant currents combined with resistance of the system make power usage one of the primary costs of operating an electrodialysis system [9].

The previously mentioned systems introduce chemical potential to a system with increased pressure (reverse osmosis) or potential (electrocoagulation, electrodialysis) while ion exchange is driven by differences in concentration. Ion exchange systems are less technically complex, but require more chemical usage. The primary drawback of ion exchange results from the addition of concentrated chemicals, because secondary treatment is required for the waste stream. These solutions are usually strong acids, strong bases, or brines which complicate subsequent treatment and reclamation of metal contaminants. Because metal contaminants cannot be degraded, reclamation represents the most sustainable endpoint. This research will examine an approach to reduce treatment requirements for secondary metals waste while avoiding significant power costs.

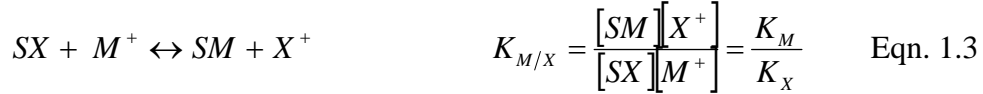
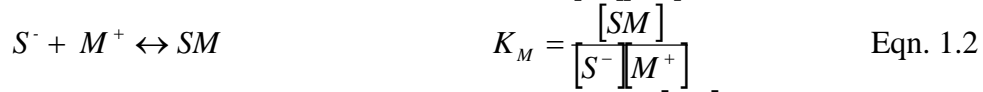
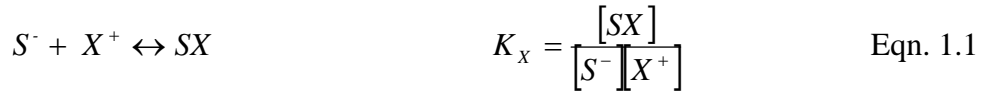
2.2 MODIFICATIONS TO ION EXCHANGE

Significant improvements have been made to ion exchange processes over the past several decades to optimize removal of metal contaminants while minimizing the concentration of regenerant chemicals required to restore the capacity of the resin. The chemical character of the resin and attached functionalities determines these characteristics of that resin. Common ion exchange resins are often composed of zeolite minerals or polymer resins. Both of these substrates have high specific surface areas, many sites for metal ion adsorption, and can be chemically modified to change adsorption character. Zeolites have significant cation exchange capacities and can be functionalized with organic ligands to change adsorption properties. The adsorption of positively charged organic molecules to a zeolite surface allows for the adsorption of not only other organic molecules but also selected anions [11]. Polymer resins provide a flexible foundation for an ion exchange process to be designed. A chemical resistant resin can be chosen for a specific application and a variety of functional groups can be attached. The functional groups provide metal binding capacity and often a degree specificity. Common categories of functional groups and examples are listed in Table 2. The relative strength of a group for a given metal is discussed in the next section.

Table 2. Common categories of functional groups found on ion exchange resins

Category	Example Group
Strong Acid	R-SO ₃
Weak Acid	R-COOH
Strong Base	R-NH ₃ OH
Weak Base	R-NH ₂
Metal Chelating	R-EDTA-Na

The ESIE process takes surface modification and functional group design on a porous medium from existing ion exchange and employs electrochemistry for the purpose of changing the metal binding character of the surface. The primary requirements for the binding functionality are affinity for the contaminant of interest and a means to overcome that affinity in order to regenerate the resin. If a binding group binds too strongly to a metal, then a large concentration of the regenerating chemical will be required to displace the metal as illustrated in following equations where S is a site where a metal or regenerant ion can bind, Me is the metal of interest and X is regenerant ion.



The term $K_M/K_X = K_{M/X}$ is known as the selectivity of the site for a specific ion M^+ over the regenerant ion X^+ . The equilibrium shown in eqn. 1.3 is the governing relationship of ion exchange. Selectivity depends on the valence and acid-base character of the ion, the type of resin, its saturation and ion concentration. It is generally only valid over a narrow range of pH [9]. Approximate selectivity values for a strong acid ion exchange resin are shown in Table 3.

Table 3. Approximate relative selectivity values for a strong acid ion exchange resin [9]

Cation	Selectivity	Cation	Selectivity
Li ⁺	1.0	Co ²⁺	3.7
H ⁺	1.3	Cd ²⁺	3.9
Na ⁺	2.0	Ni ²⁺	3.9
K ⁺	2.9	Mn ²⁺	4.1
Mg ²⁺	3.3	Ca ²⁺	5.2
Zn ²⁺	3.5	Pb ²⁺	9.9

When $K_{M/X}$ is large metal binding is strong and a significant concentration of the regenerant ion X^+ is necessary to produce a shift in the population of sites from metal-bound (SM) to regenerated (SX). A condition where $[SX]/[SM]$ is much greater than 1 requires that ratio of free regenerant to free metal is larger than $K_{M/X}$ as shown in Eqn. 1.4.

$$\frac{[SX]}{[SM]} = \frac{[X^+][M^+]}{[K_{M/X}]} \quad \text{Eqn. 1.4}$$

The requirement of a significant concentration of $[X^+]$ to regenerate is the primary reason that ion exchange waste streams are brines or strong acids or bases. A reduction in the required regenerant concentration is one of the indirect goals of this research. To achieve this goal a reexamination of eqn. 1.3 is required. The selectivity of the system is a constraining factor, because a high selectivity is desired when removing metal from the original treatment stream, but a low selectivity is desired when releasing metal back to the waste stream. The selectivity is defined by the individual equilibrium relationship between the site, metal and regenerant ion. Changes in these relationships require

changes in the complexation chemistry of the system. If the complexation chemistry and thus selectivity could be shifted for binding and non-binding situations, a proportional reduction in regenerant concentration required could be achieved. In addition to changes in selectivity, a shift in the total number of sites available could reduce the amount of metal bound directly by adding a new site-consuming reaction to the system and taking X^+ to be a proton as shown in eqn 1.5.



The ESIE system provides a chemistry framework for this change to take place through the use of redox active peptides as a binding functionality. An applied potential can oxidize or reduce these functionalities on the surface of the resin and change the selectivity and number of available sites. A further examination of potential-modified ion exchange and metal binding peptides is required to understand chemistry underlying this transition.

2.2.1 Electrochemically Switched Ion Exchange systems

The concept of using changes in potential to change the nature of the metal-surface interactions has been established in the literature. A potential applied to a conductive ion exchange resin can create an electrochemical change in pH at the surface of an electrode and the resulting pH change can increase or decrease the binding affinity of a chemical group on the surface of the electrode [12]. This concept relies on the breakdown of water and does not provide a lasting change in the nature of the electrode, as the pH gradients begin to dissipate when the potential is removed. Columns packed with graphitic carbon coated with polyvinylferrocene and polypyrrole were used to provide better chromatographic separation of pharmaceuticals [13] and substituted

phenols [14]. Work on electrochemically modulated separation on graphitic carbon was extended to common inorganic anions such as nitrate, chlorate, and bromate [15]. The majority of electrochemically modified column techniques used a continuously applied potential and changes in the distribution of ions in the double layer at the surface of the electrode to increase retention of certain molecules.

Several researchers have used electroactive molecules at the surface of an electrode to produce a persistent change in binding character. In the process of improving liquid column chromatographic techniques, potentials were applied to a conductive substrate with a polypyrrole-functionalized surface to produce a change in binding [16]. A separate example uses hexacyanoferrates deposited on the surface of a nickel electrode. These molecules are electroactive as Fe(II) is oxidized to Fe(III) at the nickel surface. Hexacyanoferrates are selective cesium binders and changes in the potential were used to load and unload cesium from the surface of the electrode [17, 18]. Electrochemical control has also been used to tautomerize 8-hydroxyquinoline adsorbed to an electrode surface for the purpose of changing metal binding characteristics [19]. These techniques more closely resemble the process scheme proposed for ESIE, where a semi-permanent electroactive modification is performed on the surface of the electrode.

2.3 METAL BINDING PEPTIDES

2.3.1 Polypeptides

The study of metal binding by polypeptides originated with evaluations of proteins in nature which chelate metals to produce functionality. These proteins form strong selective metal binders in a cellular environment. Secondary and tertiary structure in the proteins allow for multiple amino acids to coordinate around a metal. A significant fraction of enzymes require the presence of an inorganic ion in order to function [20].

Within a cell these proteins are used in processes such as direct adsorption and phytoremediation to extract and concentrate metals [21-23]. The specific metal ion required by the protein for function is usually specific. For example, in the case of hemoglobin, a single Fe^{2+} ion is coordinated by several nitrogen groups in a porphyrin ring [24]. The specificity for a certain inorganic ion is provided by the exposed functional groups in the protein. Carboxylates (in glutamate and aspartate), amines (in lysine), and thiols (in cysteine) show affinity for several transition metals [25]. One group of proteins of interest to this research is metallothioneins. These proteins are distinct because they contain a large fraction of cysteine residues which form strong complexes with soft acid metals such as lead or cadmium. Metallothioneins do not have complex tertiary structure like many other proteins, but do form secondary structures in the presence of metals. These proteins can chelate multiple metal [26].

Metallothioneins can also participate in redox chemistry which alters the metal binding capacity. Mammalian metallothioneins can undergo a thiol disulfide exchange with glutathione that transforms the binding affinity for zinc by several orders of magnitude [27].

When removed from the cellular environment, these proteins often denature and lose their binding affinity [28]. Several researchers have studied methods to isolate the binding active portions of proteins and still maintain the functionality seen in a full protein [29]. Reducing the size and complexity of the protein can reduce the selectivity and metal binding strength, but also allows the protein to function in harsher environments. An extension of this idea is to engineer proteins specifically for metal binding from amino acids. Modifications can be singular in nature [30] or encompass a large portion of the protein [31]. Changes in functionality at a specific location in a protein can create significant differences in metal binding affinity. A weak Ca^{2+} binding

site in bacterial Subtilisin showed a six fold increase in Ca^{2+} affinity after specific proline and glycine residues were changed to aspartic acid residues [30]. Short sequences of amino acids or polypeptides can provide metal binding similar in nature to larger proteins [2]. The rationale for design of metal binding peptides begins with the properties of the individual amino acids.

The simplest polypeptide is a homopolymer of a single amino acid. Existing work on poly-L-aspartate [32-34], poly-L-glutamate [34, 35], poly-L-histidine [36], and poly-L-cysteine (PLC) [3-5, 37-39] has shown significant metal binding ability in homopolymers. The structures of cysteine and PLC are shown in Figure 2.

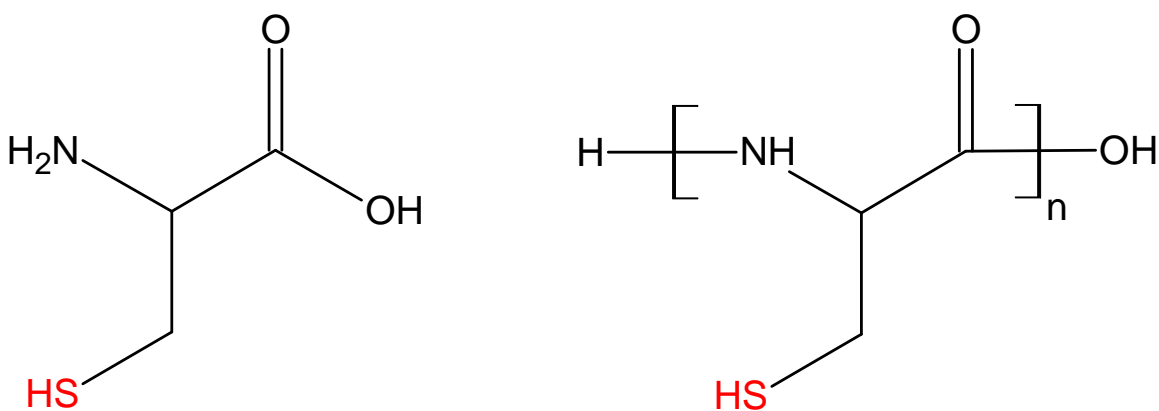


Figure 2. Chemical structure of cysteine and poly-L-cysteine (PLC)

Carboxylic acid functional peptides show general transitional metal binding, the imidazole group of poly-L-histidine binds metal anions such as arsenate, and the thiol functionality of PLC binds transition metals with an affinity for soft acid metals such as lead, cadmium, and mercury, while showing little affinity for alkali and alkaline earth metals [38]. Homopolymers are relatively simple and inexpensive to synthesize, but still provide secondary structure to allow for metal coordination. The polypeptides can wrap around a metal to increase coordination and reach a free energy minimum [33]. The coordination provides strongly binding locations within the polypeptides which have

formation constants on the order of $\log K = 13$ for poly-L-aspartic and poly-L-glutamic acid [34].

More complex peptides can be generated by mixing and matching amino acid groups. Binding properties that might not be possible with a single amino acid could be created by alternating or patterning amino acids. The design for complex multiple amino acid interaction with a single metal follow existing patterns in nature [40]. Current approaches include copying small known metal binding sequences or generating a combinatorial library of peptide sequences and screening the library for increased metal binding [35].

2.3.2 Structure and binding of polypeptides

The secondary structure of a polypeptide is dictated by its amino acids and the environment surrounding the peptide. Structures commonly seen in proteins such as helices and sheets can be formed by homopolymers and influence binding [33]. These structures promote binding by providing locations for multiple amino acids to interact with individual metal ions. A polypeptide also provides a flexible backbone for the active parts of the amino acid to move in space and surround a metal ion in a manner similar to a structured protein. The presence of a metal ion can stabilize an unstructured protein as multiple amino acids groups coordinate a single metal [33]. In addition, the state of many amino acids is altered by changes in acid/base or redox conditions. For example, redox changes affect structure in peptides containing cysteine when two cysteine molecules form covalent disulfide bonds [3]. The protonation and redox state of an amino acid affect its interaction with neighboring amino acids in a chain and have significant effects on the secondary structure of the peptide and on metal binding.

The ability to affect secondary structure by manipulating pH and redox conditions form the basis of a bind and release system for metals treatment in a manner similar to

existing ion exchange processes. Traditional ion exchange processes use an increase in a secondary ion concentration to displace the ion of interest. The secondary ion can be provided by an innocuous metal, such as sodium, or by an excess of hydrogen ions through a pH change. Acidic conditions can significantly lower equilibrium binding as protons displace metals and increase metal solubility. In either case, the metal of interest is released by changing the environment of the binding moiety. Polypeptides have the ability to provide more specificity in binding and more sophisticated methods of releasing metals.

A peptide containing multiple cysteines can be oxidized to reduce the number of thiols available for binding, since the disulfide form of cysteine binds significantly less than the thiol form as shown in the Figure 3 below [3].

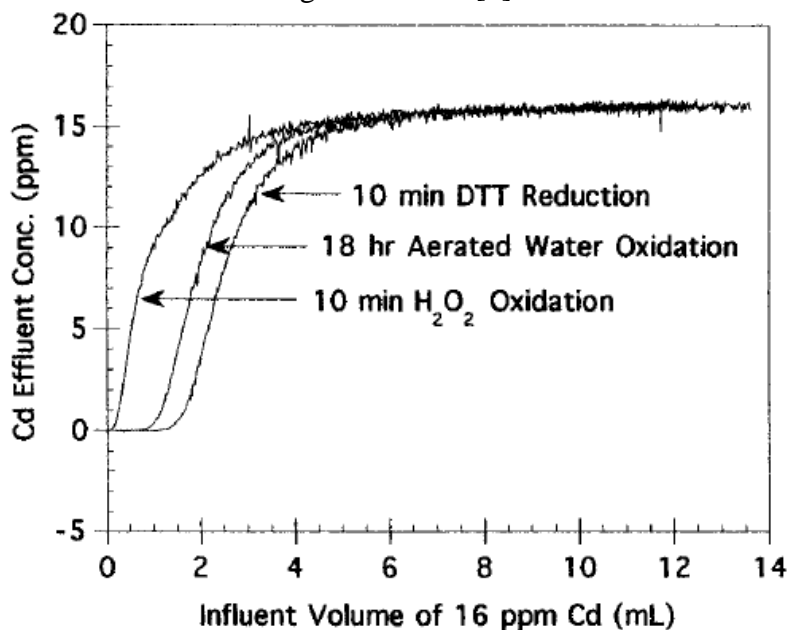


Figure 3. Breakthrough curves for Cd^{2+} at pH 7 on a PLC functionalized controlled pore glass column. Increased area above the breakthrough curve implies greater binding capacity. (Reprinted from Howard) [3]

In addition to the reduction in the number of available amino acids for binding, the creation of disulfide bonds affects the secondary structure of the polypeptide and

effectively closes up its structure. The oxidation and reduction of PLC on a glassy carbon electrode has been performed with moderate potentials of -0.6 V to +0.6 V vs Ag/AgCl, and a cyclic voltammetric analysis showed oxidation and reduction waves at 0 and +0.4 V vs Ag/AgCl respectively [6]. The redox change in cysteine provides an opportunity to affect binding affinity without significant changes in chemical composition of the environment through the application of a potential to the peptides. This allows for the release of metals without the use of high salt or acid concentrations.

Chapter 3: Design and analysis of a bench scale ESIE apparatus

3.1 GENERAL DESIGN REQUIREMENTS FOR A BENCH SCALE ESIE SYSTEM

A lab scale apparatus for ESIE experiments should provide a variety of options for testing the chemical properties of the peptide modified substrate and provide insight to the design and construction of a larger scale system. The design of the system considered two main requirements:

1. The ability to oxidize/reduce the substrate by applying a potential, and
2. The ability to assess the capacity of the substrate for particular metal ions

Based on a comparison of the previous research conducted with PLC and to other competing technologies, one of the key objectives of this research was to develop a system which could treat water at laboratory scale (0.1 to 1 L of water at 1 to 10 mg/L contaminant concentration).

This chapter describes selection and preparation of the substrate and peptide and the physical design of the ESIE apparatus. The methods used in synthesis and construction are described at the end of chapter. Layout and schematics of the system designed in this research are presented, and the various tests of operational characteristics of the system are explained.

3.2 EXPERIMENTAL METHODS

The methods described below were used to fabricate the ESIE system. The rationale for the methods and design of the system are described in the next section.

3.2.1 Instrumentation

Peptides were synthesized through Fmoc-solid phase peptide synthesis (SPPS) using a Ranin Symphony Quartet automated peptide synthesizer. Mass spectra of

peptides were obtained on a PerSeptive Biosystems Voyager MALDI-TOF. Either a DC power supply (Hewlett Packard) and voltmeter or three-electrode potentiostat (Cypress Systems Omni-101) were used with a Miniature Teflon Ag/AgCl reference electrode (Cypress Systems) and platinum wire counter electrode for electrochemical modification steps. Solution was pumped through the apparatus with a Carter Manostat peristaltic pump and pH was monitored with a digital pH/mV/ORP meter (Cole-Parmer).

3.2.2 Reagents

Peptides were synthesized and cleaved on Wang resin (Novabiochem) using cysteine (Fmoc-Cys(trityl (Trt))-OH) (Novabiochem), hexafluorophosphate (HBTU) (Novabiochem), and 1-hydroxybenzotriazole (98%) (HOBt) (Novabiochem), triisopropylsilane (99%) (TIPS), ethyl ether (Fisher), N-methylmorpholine (NMM) (Fisher), N-methylpyrrolidone (NMP) (Fisher), trifluoroacetic acid (TFA) (99%) and piperidine (99%). Peptides and amino acids were attached with 2-(N-morpholino) ethanesulfonic acid (MES), N-(3-dimethylaminopropyl)-N'-ethylcarbodiimide (EDC) (Sigma Aldrich), N-hydroxysuccinimide (NHS), L-cysteine and glycine. Analysis and testing procedures used acetonitrile, DL-1,4-dithiothreitol (99%) (DTT), sodium hydroxide. 5,5'-dithio-bis (2-nitrobenzoic acid) (DTNB) and tris(hydroxymethyl) aminomethane-HCl (Tris-HCl).

3.2.3 System Construction and Assembly

A homopolymer of cysteine was formed by using Fmoc based synthesis. A sequence program of 20 cysteines each coupled twice for 45 min was attached to Wang resin with a nominal loading of 0.1 mmol/g resin. The resin was removed from the synthesizer and the peptide was cleaved and deblocked using a solution of 95/2.5/2.5 TFA/TIPS/DI H₂O for 3 h. The resin was filtered and additional TFA was used to rinse

the resin. The filtrate was reduced with a stream of N₂ and then added to cold ethyl ether and allowed to precipitate for 30 min. The solution was centrifuged and rinsed with ether 3 more times. The pellet was suspended in DI water and the solution was lyophilized overnight to produce pure solid peptide.

The peptide was characterized by MALDI-TOF mass spectrometry. 1 mg of peptide was dissolved in 1 mL of 20% acetonitrile/80% DI water with 10 μ L of TFA. The solution was dried onto a spot well on a metal array with a standard matrix solution. The array was placed in the MALDI-TOF mass spectrometer and the resulting mass spectrum was recorded.

A glassy carbon electrode was fabricated as previously outlined. The carbon electrode, platinum wire counter electrode, and Ag/AgCl reference electrode were assembled with inlet and outlet pieces for circulation of reagents. DI water was passed through to rinse the apparatus. To oxidize the surface of the electrode 1 M H₂SO₄ was circulated while applying a voltage of +2 V referenced against the Ag/AgCl electrode for 20 min. The oxidation step produces active oxygen functionalities on the surface which include alcohols, aldehydes, and carboxylic acids. A carbodiimide facilitates the attachment of the amine terminus of the peptide to a carboxylic acid [37]. A 0.04 M solution of EDC with 0.06 M NHS buffered by 0.05 M MES at pH 5 was circulated through the carbon electrode for 2 h. NHS helps to stabilize a reaction intermediate formed between the surface carboxylic acid and EDC [41]. The electrode was rinsed with DI water to remove excess EDC solution. The poly-L-cysteine homopolymer was dissolved in 0.05 M MES and adjusted to pH 6. The PLC solution was then circulated overnight through the electrode to allow reaction with the EDC intermediate. The electrode was then rinsed with DI water. This process was repeated using a single cysteine and single glycine amino acid to produce cysteine and glycine electrodes. After

attaching the peptide, the electrode was put through one redox cycle to remove any sites that were not able to be reduced or oxidized reversibly. For reduction of disulfides on the electrode, 50 mL of 0.02 M DTT at pH 8 was circulated for 10 min. For oxidation of the thiols on the electrode, 50 mL 1% H₂O₂ was circulated for 10 min.

3.2 SUBSTRATE PREPARATION

3.2.1 Substrate material selection

The requirement of a surface bound, electroactive polypeptide places several constraints on choice of substrate. The substrate needs to be conductive and capable of carrying enough current to oxidize and reduce the peptide on the surface, while being electrochemically inert itself. The peptide needs to be attached to the substrate covalently and with sufficient strength that no peptide is lost with the oxidizing or reducing potential applied to the system. Previous work used a glassy carbon disk electrode which meets the chemical requirements but with a small capacity - 100 ng of Cd²⁺ on a 0.25 cm² surface at an equilibrium concentration of ~10 mg/L [6]. A substrate with a greater specific surface area is necessary to scale the ESIE process for continuous flow processes at laboratory, pilot, and full scale systems.

Reticulated Vitreous Carbon (RVC) was chosen as the substrate material for the ESIE system after analysis of several options commonly used as electrode materials or ion exchange resins. Metal based substrates are susceptible to oxidation at positive potentials or corrosion in the presence acids or salts. Glass and polymer substrates are either insulating or have relatively low conductivity. Carbon, as used for the disk electrode in previous work [6], met all the necessary requirements. Initial experiments used microporous activated carbon samples. Activated carbon fiber woven cloth was obtained and several surface analyses were performed to assess its performance in an

ESIE system. BET surface area was estimated at $1600 \text{ m}^2/\text{g}$, though not all of the area was accessible to the ESIE process. A significant portion of the surface area was contained in microporous structure. Based on estimations derived from Miller, a 10-mer of PLC has a lower limit on characteristic length of $\sim 4 \text{ nm}$ in solution [5]. If it is assumed that a pore must have a diameter greater than 4 nm for the area contained within to be accessible to a PLC molecule, then all pores less than 4 nm in diameter have an area which would not be included in the ESIE scheme. The area of pores greater than 1.7 nm in diameter was $\sim 250 \text{ m}^2/\text{g}$ by BJH adsorption. At least $1350 \text{ m}^2/\text{g}$ of pore area would be inaccessible to the ESIE process, but still available for non specific metal ion adsorption. Electrolyte ions in solution can access the microporous area and associate with the double layer at the surface of the electrode when a potential is applied. In fact, this property is exploited in the use of activated carbons as the substrate in electrochemical capacitors [42]. Cyclic voltammetry (CV) of the activated carbon cloth confirmed this by showing extremely high capacitive currents.

shows no faradaic peaks as the capacitive current is likely several orders of magnitude greater than any faradic current. An increase in potential on the surface of an activated carbon necessitates a significant amount of current to form an ionic double layer at the surface [42]. For this reason, other carbon substrates were evaluated. Graphitic carbons and glassy carbon beads meet the majority of the requirements for an ESIE electrode, but present another challenge. Particle based electrodes require a method of containment which permits flow, provides a good conduction path and minimizes distance to the counter electrode. Reticulated Vitreous Carbon (RVC) is chemically similar to glassy carbon but is monolithic, which provides a significant advantage in terms of system complexity and handling of electrode materials. For this reason RVC was selected over the other chemically equivalent carbons. A summary of the substrate

material options and reasons each was dropped from consideration in the ESIE system is presented in Table 4.

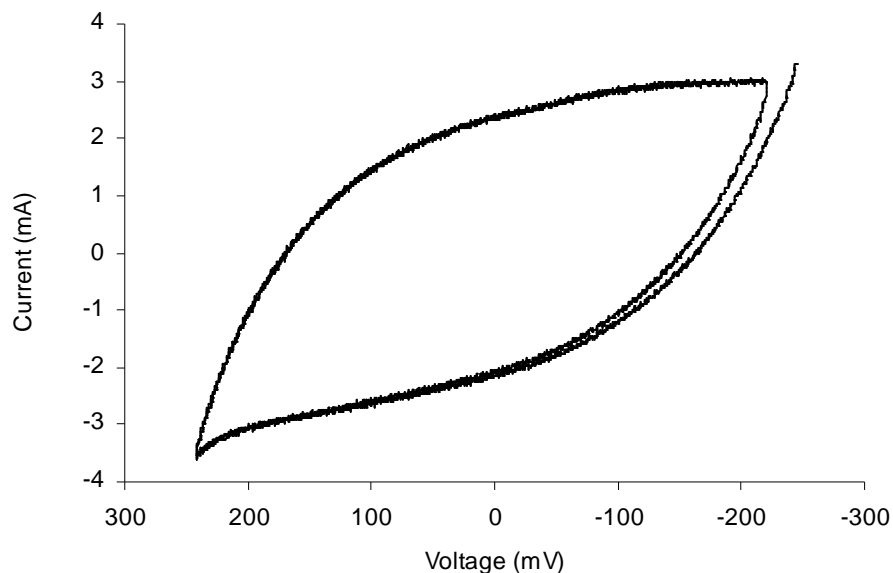


Figure 4. Cyclic Voltammogram of a cysteine functionalized activated carbon cloth in 1 M H_2SO_4 . Carbon mass = 10 mg, Scan Rate = 1 mV/s

Table 4. Substrate Material Options

Substrate	Reason not considered
Metal	Oxidation by ESIE electrochemistry Corrosion by strong acids or salts
Glass Plastics	Not conductive
Activated carbon	Large capacitance Non specific adsorption
Graphitic carbon	Containment and handling
Glassy carbon beads	Containment and handling

Layout of the system is discussed later in this section. RVC provides a monolithic substrate with surface area comparable to a packed column of small glassy

carbon particles. Since the carbon consists of a single piece of material, contact resistance between particles and containment problems were circumvented. Nine hundred ppi (pores per linear inch) RVC foam was obtained from ERG Aerospace (Oakland, CA) for use in the ESIE apparatus. [43, 44]. A list of physical properties of 900 ppi RVC is shown in Table 5. Examples of RVC foam are shown in Figure 5.

Table 5. Physical properties of 900 ppi Reticulated Vitreous Carbon [43]

Property	Value	
Bulk density	0.45	g/cm^3
Carbon density	1.49	g/cm^3
Porosity	0.70	
Specific Area	1320	cm^2/g
Area per unit volume	590	cm^2/cm^3
Bulk Resistivity	5×10^{-3}	$\Omega\text{-cm}$

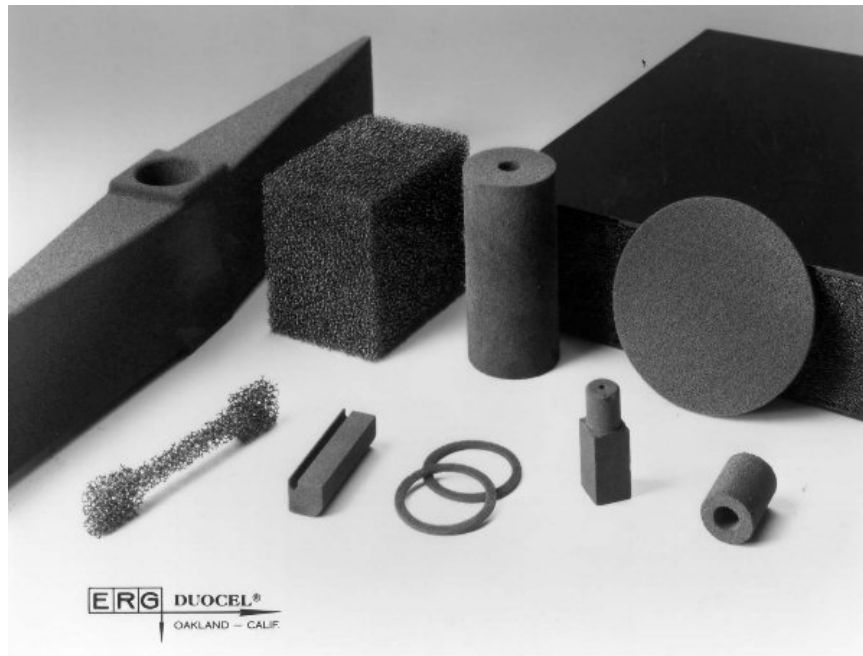


Figure 5. Examples of Reticulated Glassy Carbon foams from ERG Aerospace [45].

3.1.1 Peptide attachment

The ESIE system is predicated on the ability to switch binding through the oxidation of cysteine functional groups. A PLC functionalized electrode was built to test properties of the ESIE system. PLC was the primary peptide studied, but cysteine and glycine were used for certain tests. Cysteine monomers represent the simplest redox active peptide system. Glycine represents a control for the electrode surface and binding ability of the terminus of the peptide.

The PLC was generated with the use of a peptide synthesizer and characterized by MALDI-TOF mass spectrometry. The resulting mass spectrum is shown in Figure 6. The peptide was created stepwise by successive additions of cysteine. Each addition has an efficiency less than 100%, so a distribution of peptide lengths results. For this PLC, the peptide length ranged from 7 to 11 cysteine residues.

A carbodiimide linker was chosen based on use in previous work [6]. For a carbon substrate a strong oxidation potential can be used to produce carboxylate functionality at the surface. The carboxylate functionality provides an attachment point for the peptide. The peptide is bound to the surface through the reaction of surface carboxylate reacted with the amine terminus of the peptide through the use of the carbodiimide linker (EDC). A schematic of the process of peptide attachment is shown in Figure 7.

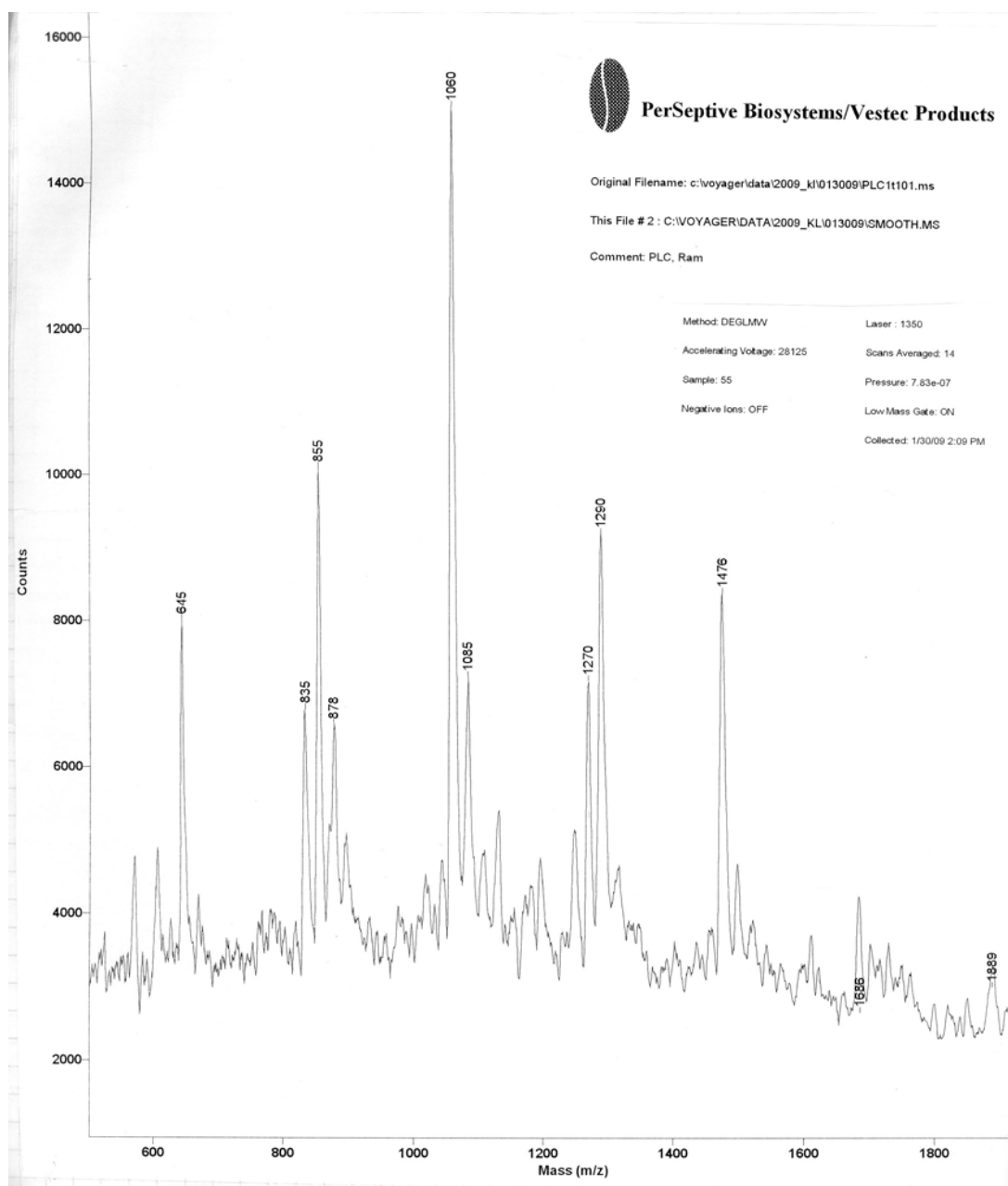


Figure 6. MALDI analysis of synthesized PLC peptide.

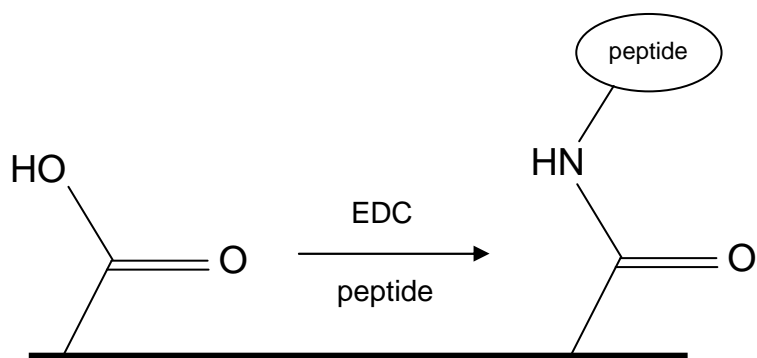


Figure 7. Peptide immobilization reaction. Carboxylate functionality on the substrate reacts with the N-terminus of a peptide using EDC to facilitate the reaction

3.3 SYSTEM DESIGN AND LAYOUT

3.3.1 System Requirements

The substrate needs to be contained within a system that allows for electrochemistry and adsorption experiments in a convenient manner. Much of the complexity of the system comes from the nature of the electrochemical setup. The substrate serves as a working electrode, and a reference electrode needs to be kept in proximity to the working electrode to reduce the error in measured potential at the working electrode. The counter electrode should also be kept as close as possible to the working electrode to reduce resistive losses in solution. Current through the system flows through the solution gap between the working and counter electrode, and increased distance creates increased resistance [46]. Increased resistance leads to increased power usage for the redox switch in the system. The porous nature of the substrate increases the average distance between the surface of the substrate and the counter electrode. This problem can be reduced by fragmenting the working and counter electrode into several parts and staggering them within the system, although this increases system complexity. The substrate needs to be electrically connected to a power supply or potentiostat, and the connection should be stable in the changing environment within system. All components

of the system are exposed to significant acid concentrations for short periods of time and moderate acid and salt concentrations for extended periods of time. The structure containing the electrodes should be electrically insulating and water tight to allow for low pressure flow through the system.

Because of the high surface area of the substrate, pressurized flow is necessary to reduce mass transfer limitations within the system. Batch equilibrium tests require that the time scale of mass transport be significantly smaller than the time scale of the entire equilibrium experiment. If the substrate is microporous, then diffusion through pores can be limiting, and a mass transport analysis will be required. The substrate can either be monolithic or particle based, and there are considerations for each case. A monolithic substrate will need to be machined to a proper geometry and a particle based substrate will need to be contained in a convenient manner inside the setup. Electrical contact resistance between particles should be insignificant compared to the other resistances in the system. A drawback of a particle based setup is the difficulty in segmenting the substrate, as each segment would require its own containment.

The system should be flexible to allow for several types of adsorption experiments. Batch equilibrium experiments will comprise the majority of the analysis of the system. Batch experiments require the system to contain a well-mixed solution reservoir while maintaining flow around the substrate. Rate experiments could use a similar setup if the reservoir can be periodically sampled while adsorption is taking place. A column based experimental setup would ideally utilize pressurized one-dimensional flow across the substrate without significant axial mixing.

3.3.2 System Design

The primary challenges of system design included electrode placement and pressurized flow through the system. A modular enclosure system was developed as a

solution to both problems. RVC foam was machined into cylinders approximately one inch in diameter and 1/8 inch thick. These cylinders were then placed inside a larger plastic disc housing containing a platinum contact wire for connection between the RVC and a power supply. Conductive epoxies were considered for better electrical connection, but most epoxy formulations contained electroactive constituents (e.g., silver) which would react under the range of conditions seen inside the system. The seam between the RVC cylinder and the plastic disc housing and the location where the contact wire entered the inside of the housing was sealed with a silicone sealant. The channel for the wire was sealed on the outside of the housing with epoxy to bear loads induced by alligator clipped connections. The first few parts were machined from Delrin, but it was found to decompose after extended exposure to acid. Further parts were machined from Teflon, and the system was stored without acid present. Discs were also constructed to house the platinum counter electrode and Ag/AgCl reference electrode. The platinum counter electrode wire was coiled in the center of the plastic disc housing and sealed in the same manner as the working electrodes. The discs were placed on top of each other in any order to form a complete electrochemical cell. The gap between each disc is sealed by an o-ring. Also since the system is modular, additional discs can be added to the system to increase substrate area or stagger counter electrodes between substrate discs to reduce resistive losses. Influent and effluent caps were made to match the discs and channel flow through the system. Design drawings of the parts are shown in Figure 8 through Figure 11. The outlet is the same as the inlet, except for the omission of the o-ring groove. The primary components of the system are shown in Figure 12.

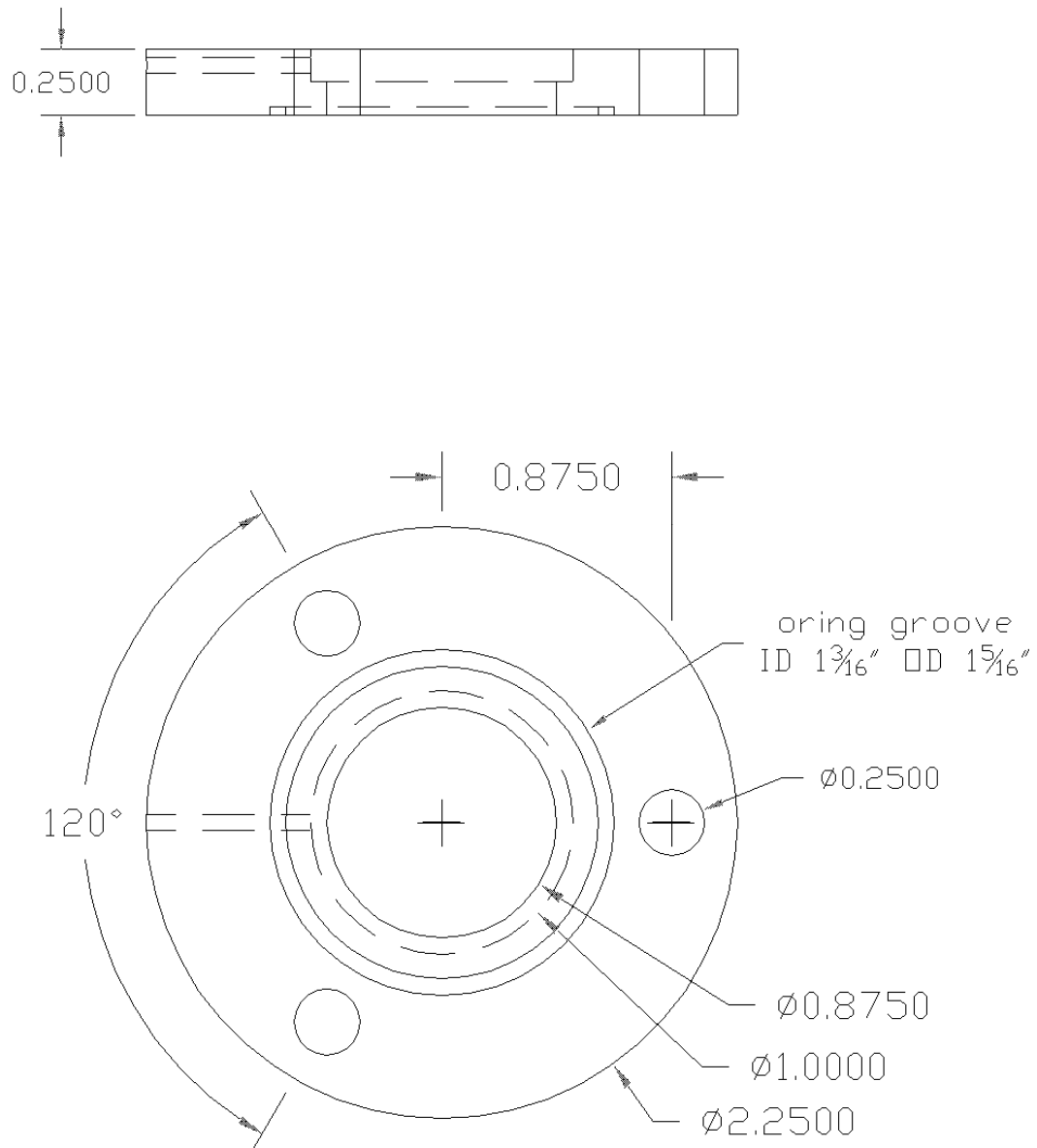


Figure 8. Top and Front views of the electrode housing

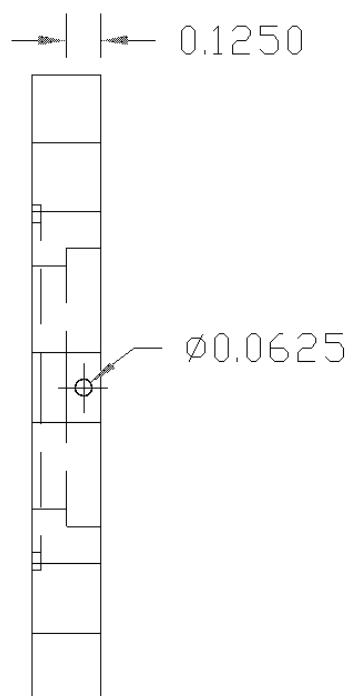
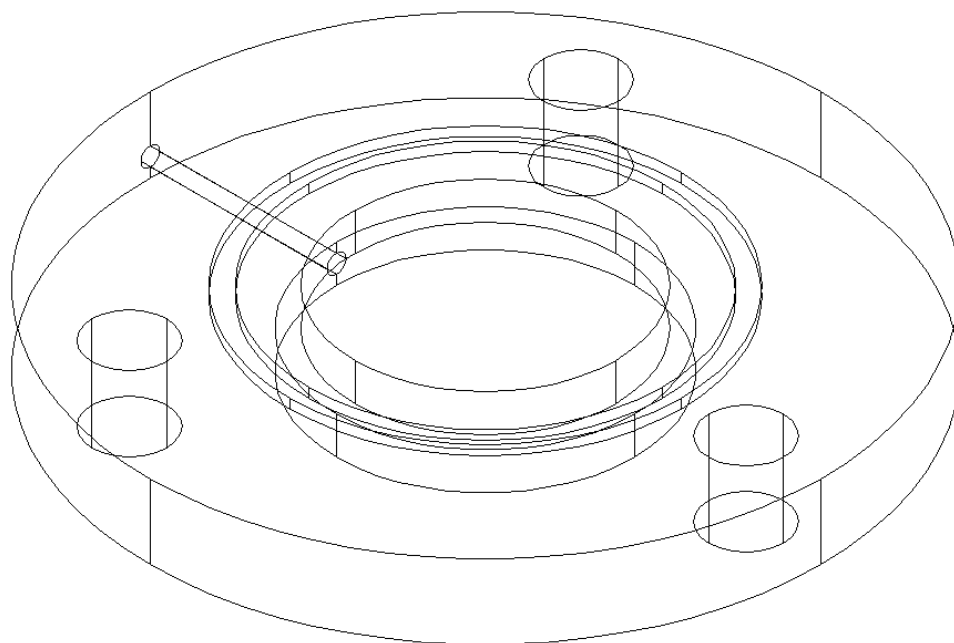


Figure 9. Side and wireframe isometric views of the electrode housing

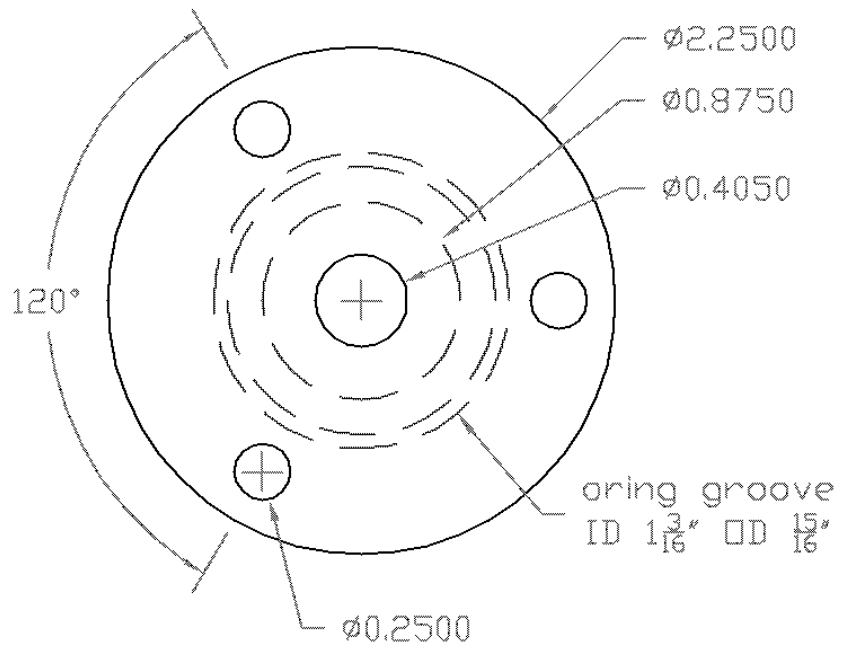
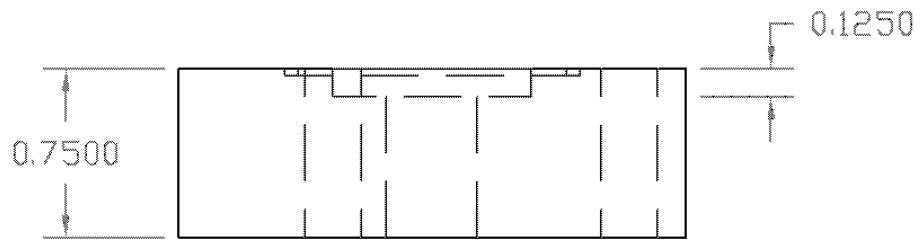


Figure 10. Top and front views of the inlet.

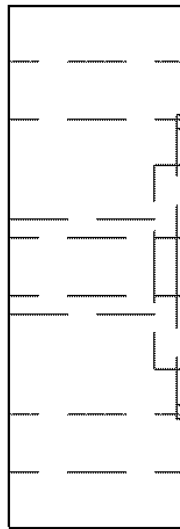
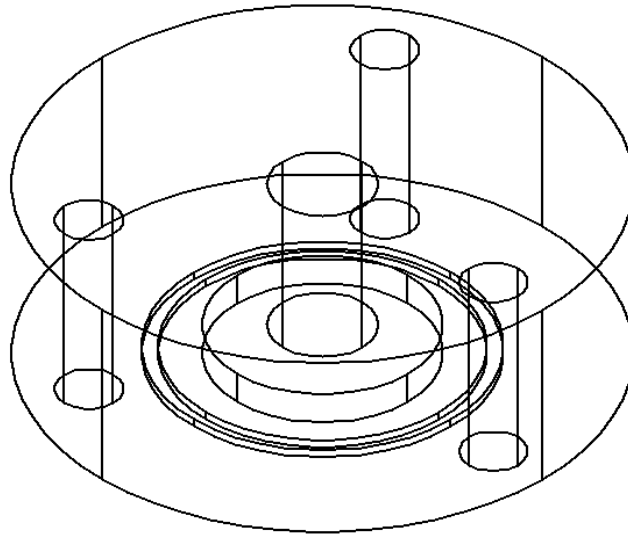


Figure 11. Side and wireframe isometric views of the inlet

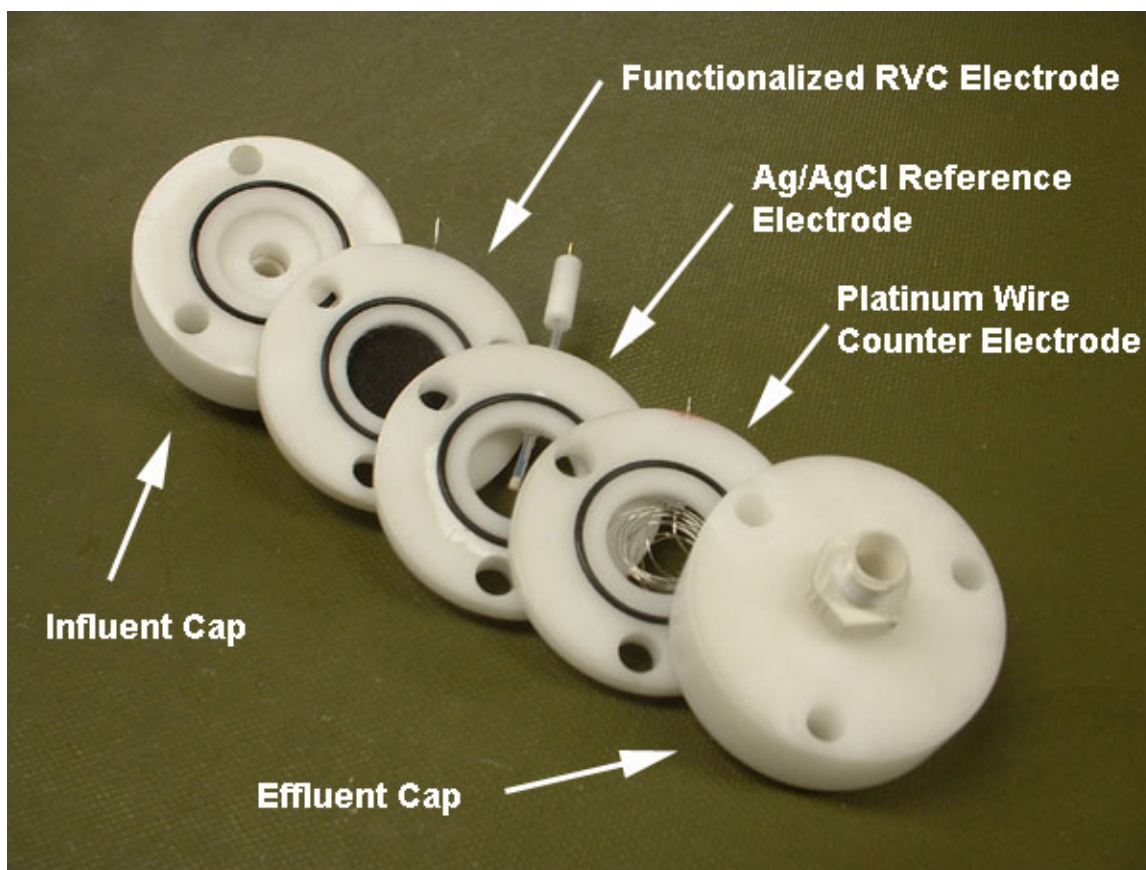


Figure 12. Primary components of the lab scale ESIE system

A single disc with RVC substrate has a surface area of 950 cm^2 within a volume of less than 2 cm^3 . The volume of the system with three empty discs is approximately 13.6 mL . The electrode discs and end caps are compressed together with three bolts to seal the assembly. Influent and effluent tubing are attached to threaded connectors at the two end caps. Fluid is pumped through the system by a peristaltic pump. To increase the working volume of the system, a well mixed external reservoir is used to store the feed solution and to allow recirculation of the effluent through the system. Solutions are kept oxygen free by sparging with nitrogen gas, and pH is continuously monitored by a probe immersed in the reservoir. The three electrode discs are connected to a potentiostat or

power supply. Figure 13 shows the layout of the ESIE system used for bench scale analysis.

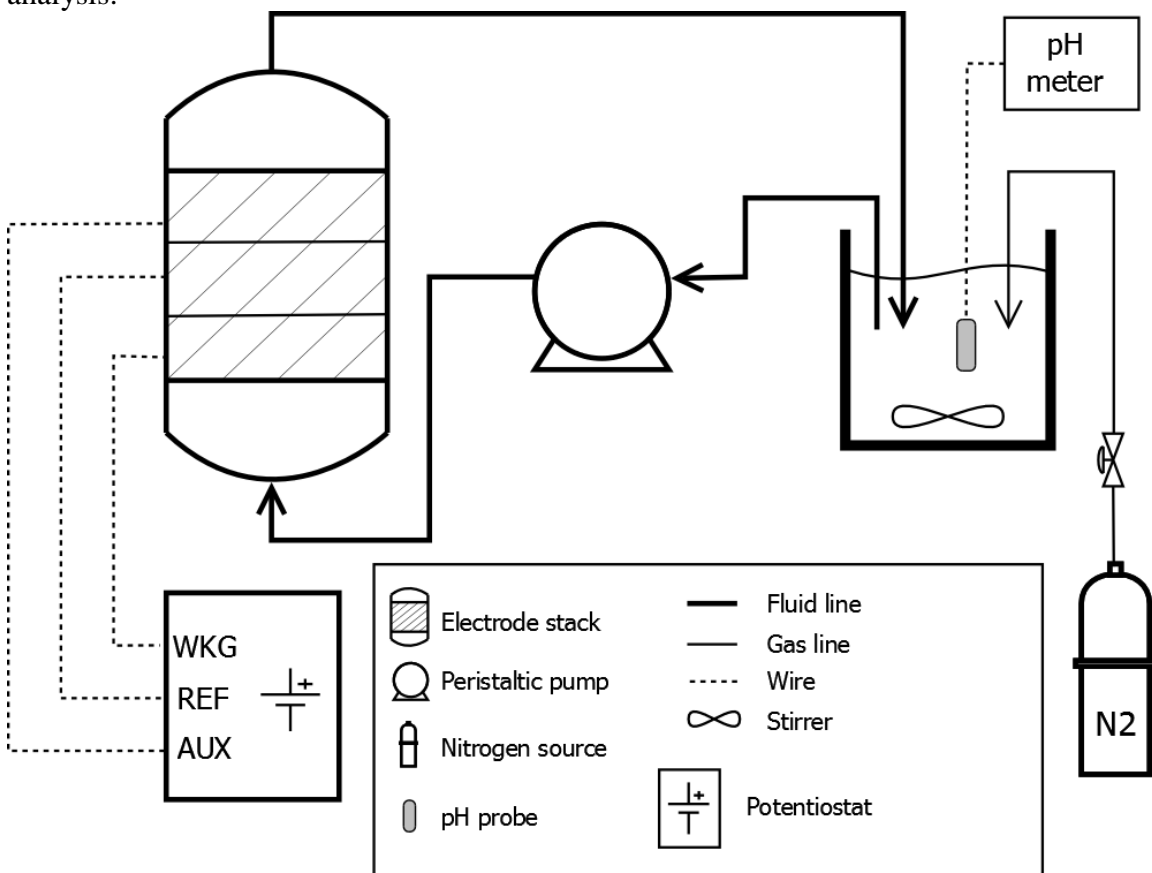


Figure 13. ESIE System Schematic

3.4 ELECTROCHEMICAL CHARACTERISTICS

A series of potential step experiments were run to characterize the current required to oxidize or reduce the PLC-RVC electrode. The experiment was procedurally the same as the electrochemical oxidation and reduction mentioned in the following chapter except that three different electrolyte concentrations were tested: 0.05 M, 0.2 M and 1 M KCl. The potential was stepped to -800 mV or +800 mV vs Ag/AgCl, and current was monitored over time until a steady current was reached. The reduced and oxidized potential steps are shown in Figure 14.

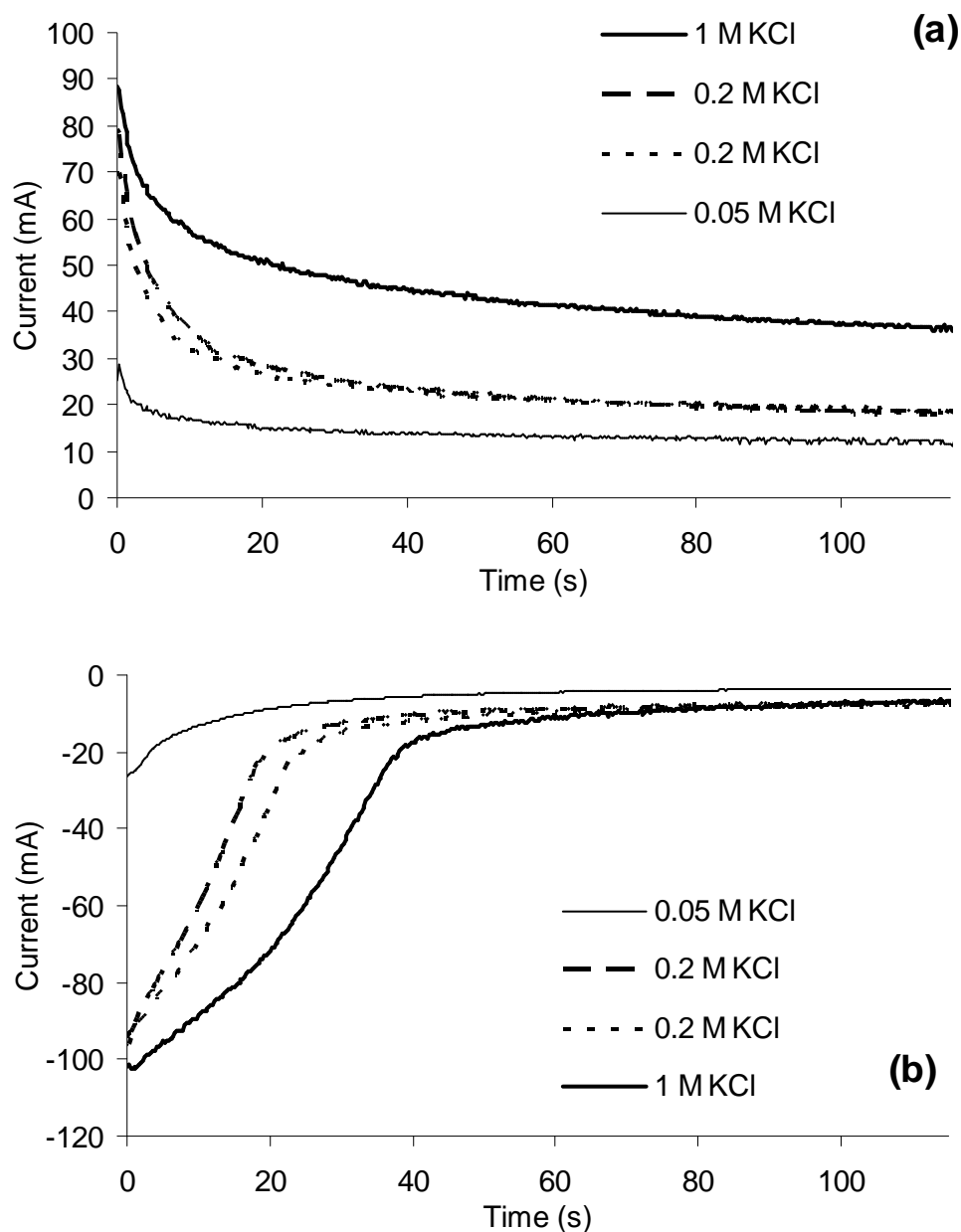


Figure 14. Current usage for electrochemical reduction (a) and oxidation (b) of RVC-PLC at -0.8 V and +0.8 V vs Ag/AgCl with 0.05, 0.2 and 1 M KCl

Both reduction and oxidation steps show expected trends of increasing current with increasing ionic strength. The relationship between conductivity in solution and ionic strength is proportional for ideal solutions [46]. Increased conductivity produces

increased current. Initial reduction and oxidation currents are comparable in opposite directions, but the steady state reduction current is significant, especially at high ionic strength. This indicates that there is a component of the solution which is being reduced at -0.8 V vs. Ag/AgCl. The total current delivered after 1 min can be used to estimate the current required when scaling up the ESIE process. While geometry plays a large role in determining the cell resistance and thus current, an order of magnitude estimate is possible for larger systems if a similar design is employed.

Chapter 4: Metal adsorption on the ESIE apparatus

This chapter examines metal cation adsorption on the ESIE apparatus to evaluate the binding capacity and elucidate the mechanisms of binding of the ESIE substrate in both oxidizing and reduced environments. The analysis included batch equilibrium experiments and spectroscopic measurements of equilibrated samples. First, a preliminary rate experiment was conducted to establish the time necessary for the system to return to equilibrium after a perturbation. pH adsorption edge and isotherm experiments were conducted using a series of oxidation and reduction methods to establish the nature of the binding mechanism and capacity of the electrode. X-Ray Absorption Spectroscopy (XAS) analysis of the oxidized and reduced electrodes was performed to provide information on the coordination environment around the adsorbed metal ions. Molecular scale observations from Extended X-Ray Absorption Fine Structure (EXAFS) analyses were used to support hypotheses established in the ESIE bench scale experiments. The results and analysis follows a description of the methods used for experimentation

4.1 METHODS

4.1.1 Instrumentation

The ESIE apparatus as constructed in Chapter 3 was used to conduct all rate and equilibrium experiments described in this chapter. Cd^{2+} and Ni^{2+} concentrations were measured by an atomic absorption spectrometer (AA-875, Varian) or inductively coupled plasma - time of flight - mass spectrometer (ICP-MS-TOF) (Optimass 8000, GBC Scientific). pH measurements were made with a digital pH/mV/ORP meter (Cole-Parmer).

4.1.2 Reagents

The following reagents were used in the course of equilibrium and spectroscopic experiments: sodium nitrate, potassium chloride, sodium hydroxide (standardized), HEPES (N-[Hydroxyethyl]piperazine-N'-[2-ethanesulfonic acid]) (Sigma), DTT (DL-1,4-dithiothreitol), 99% (Fisher), Hydrogen peroxide, 30% solution (Sigma Aldrich), 70% nitric acid, trace metal grade (Fisher), nickel(II) nitrate hexahydrate, cadmium nitrate tetrahydrate Puratronic solids (Alfa Aesar), and Cd, Ni atomic absorption standards (Inorganic Ventures)

4.1.3 Rate Analysis

The primary purpose of the rate study was to establish the time for the system to reach equilibrium after a perturbation. A metal containing solution was circulated over a metal-free electrode, and metal concentration was monitored over time. An electrode was prepared by rinsing it with 0.1 M HNO₃ to establish a baseline metal-free electrode. The acid solution was rinsed out of the system by running several bed volumes of DI water through the apparatus. The electrode was then reduced by circulating a 0.02 M DTT solution that was adjusted to pH 8 for 20 min as established in previous literature for the reduction of immobilized PLC [3]. The DTT solution was rinsed with DI water in the same manner as the acid. O₂/CO₂ free water was prepared by boiling deionized water and bubbling with N₂ overnight or longer.

At this point, two sets of rate experiments were run with Cd²⁺ and Ni²⁺. The Cd²⁺ rate experiment used a 50 mL solution of 5 mg/L Cd buffered with 10 mM HEPES (pK_a = 7.55) at pH 7. The glycine, cysteine, and PLC electrodes were each reduced electrochemically in 0.2 M KCl at a potential of -800 mV vs Ag/AgCl. The pump rate for solution was 10 mL/min for each Cd electrode. The Ni rate experiment used a 100 mL solution of 20 mg/L Ni buffered with 5 mM HEPES adjusted to pH 7 and 50 mM

NaNO₃. At time zero, the solution was pumped through the apparatus at a rate of 30 mL/min. The initial metal concentration in both rate experiments was prepared by the addition of the appropriate volume of a 1000 mg/L atomic absorption standard in 1% HNO₃. The solution was bubbled with N₂ (50 mL/min) for 30 min prior to and during the duration of the experiment. 500 µL samples were taken at regular time intervals and diluted with 0.1 M HNO₃ for analysis by flame AA.

4.1.4 Adsorption Edges and Isotherms

The primary methods to characterize the interaction between the immobilized peptide and the metal cations are adsorption edge experiments and isotherm experiments. Adsorption edges allow for characterization of the pH dependent behavior of the peptide metal ion system and isotherms. All edge and isotherm solutions were prepared from O₂/CO₂ free water as described in the rate analysis section. All solutions were circulated at a flow rate of 30 mL/min unless otherwise specified. Metal ion stock solutions used in edge and isotherm experiments were made from high purity solids dissolved in 0.01 M HNO₃. Solution concentrations were measured directly and adsorption densities were calculated from mass balances on total metal in the system.

4.1.4.1 Electrode Preparation

Prior to each experiment, 0.1 M HNO₃ was circulated through the electrode for 10 min at 10-30 mL/min to establish a baseline metal-free electrode. A DI water rinse was then flowed for 2 min to remove remaining acid. For chemical reduction, the electrode was either reduced by circulating 50 mL 0.02 M DTT at pH 8 for 20 min or 50 mL 0.13 M NaBH₄ for 10 min [47]. Chemical oxidation was performed by circulating 50 mL 1% H₂O₂ for 20 min [3]. The electrode was then rinsed with DI water to remove traces of redox agents and immediately used in edge or isotherm experiments. For

electrochemical oxidation or reduction, 0.01 M KCl was circulated through system and a +0.8 V (oxidation) or -0.8 V (reduction) vs Ag/AgCl potential was applied to the working electrode through the potentiostat for 5 min. The current was recorded after 5 s and after approximately 2 min.

4.1.4.2 Adsorption Edges

For adsorption edge experiments, a 100 mL solution of 0.01 M sodium nitrate and 0.005 M HEPES was spiked with a stock solution of the metal of interest. The pH of the resulting solution was low (~2-3) and was used as the starting point of the adsorption edge. Nitrogen was bubbled continuously and pH was monitored. A sample was taken before contact with the electrode to provide an experimental initial concentration value.

Circulation through the ESIE apparatus was started and an initial time was recorded. After 40 min of circulation, a sample was taken and the pH was recorded. 0.1 M or 0.5 M NaOH was then used to increase the pH by 0.5 to 1 units. The system was then allowed to circulate for another 40 min while the process was repeated for increasing pH until a pH of 8-9 was reached. The maximum pH was determined by the solubility of the metal ion of interest. Desorption was performed by the addition of 0.1 or 0.5 M HNO₃ to the reservoir in the same manner as the adsorption portion of the experiment. At the conclusion of the experiment, 50 mL of 0.1 M HNO₃ was run through the system for 5 min to remove remaining metal ion adsorbed over the course of the experiment. Samples were then diluted with 0.1 M nitric acid and analyzed by Flame AA or ICP-MS-TOF with matrix matched standards.

4.1.4.3 Adsorption Isotherms

For adsorption isotherm experiments, a 100 mL solution of 10 mM NaNO₃ and 5 mM HEPES was adjusted to pH 7 with 0.1 and 0.5 M NaOH. The solution was bubbled

with N_2 and allowed to equilibrate with the ESIE apparatus. The reservoir was maintained at pH 7 over the duration of the experiment. A separate metal ion solution was created by adding 10 mL of 500 mg/L metal stock to 10 mL of 10 mM NaNO_3 and 5 mM HEPES. This solution was adjusted to pH 7 by addition of 0.1 and 0.5 M NaOH to give a solution slightly below 250 mg/L.

A sample for metal analysis was taken, and then an aliquot of the metal solution was added to the reservoir. The system was allowed to equilibrate for 40 min. At that time, a sample was taken and the pH was recorded. If necessary, a pH adjustment was made by the addition of 0.1 M NaOH and another aliquot of metal ion solution was added. The system was again allowed to equilibrate, and this process was repeated until it was believed that the substrate had been saturated with metal. At the conclusion of the experiment, 50 mL of 0.1 M HNO_3 was pumped through the system for 5 min to remove any metal ion adsorbed over the course of the experiment. A sample of the metal solution used to dose the reservoir was also taken. Samples were diluted in 0.1 M HNO_3 for Flame AA or ICP analysis with matrix matched standards.

4.1.5 XAS Procedure

In order to relate bulk measurements of adsorption capacity to molecular level reactions occurring at the surface of the electrode, the adsorbed metal was probed using x-ray absorption spectroscopy (XAS). High intensity, high energy monochromatic x-rays are focused on the sample and the absorption or fluorescence spectrum is recorded. If the x-ray energy coincides with the energy required for photoelectron ejection of the atom of interest, a sharp increase in absorption occurs. XAS spectra can be divided into two parts, x-ray absorption near edge structure (XANES) which occurs at around the edge jump, and extended x-ray absorption fine structure (EXAFS) which is a post-edge region of the total spectrum. After the jump, highly energetic photoelectrons are emitted from

central atom (element of interest) and backscattered by surrounding atoms. These backscattered photoelectrons caused constructive or destructive interferences with the outgoing photoelectrons depending on the incident energy. These interferences result in oscillations observed in EXAFS region. The nature of this scattering is a powerful tool that provides information on the coordination environment of a metal *in situ*. XANES analysis, while difficult to derive quantitative results, provides important information regarding the chemical structure of the nearest surrounding atoms. Analysis of EXAFS components give estimates of interatomic distances and coordination numbers of neighboring atoms. One of the primary advantages of x-ray absorption is that many elements can be examined at low concentrations in the presence of water and other solids at much higher concentrations. A true *in situ* measurement is important for examination of the coordination environment since the presence of water can greatly influence metal coordination. For further description of EXAFS theory see Brown [48].

XAS samples were prepared by first producing an oxidized and reduced ESIE electrode using the procedures established previously. Oxidation or reduction was performed chemically using DTT or hydrogen peroxide respectively. Following a DI water rinse the electrodes were allowed to equilibrate with 50 mL of a 40 mg/L Cd^{2+} solution buffered with 0.05 M HEPES and 0.01 M NaNO_3 . Initial and final cadmium concentrations were measured by Flame AA. Electrodes were removed from the apparatus without rinsing and sealed in air-tight containers in a glove box for shipping to the synchrotron facility, Stanford Synchrotron Radiation Lightsource (SSRL) (Menlo Park, CA). Samples were stored in a glove box at SSRL and loaded onto sample cells sealed with a Kapton tape window just prior to XAS collection to prevent any redox reactions. There is no evidence of beam induced redox during data collection since the spectra were the same among different scans of each sample. The spectra were collected

at the Cd K-edge with Si(220) monochromators. ESIE electrodes were placed at a 45 degree angle in the beam path and x-ray fluorescence signals were recorded using a solid state 32-element germanium detector. In addition, a model compound for the Cd-S interaction, cadmium sulfide, was diluted using boron nitride and its spectra were collected in transmission mode. The relatively low concentration of cadmium present within the ESIE electrode necessitated more than 10 scans for each sample, averaging several scans increased the signal to noise ratio in the EXAFS region. Monochromatic energy was calibrated with Cd foil as an internal standard placed between ion chambers inline with the sample.

4.1.6 XAS Data Analysis

EXAFS data analysis was performed with SixPACK [49] and EXAFSPAK [50] software packages. Initial XAS raw data processing was done with SixPACK. Data acquired from a 32 element fluorescence detector was averaged, and specific channels that provided consistently noisy or discontinuous data were removed from averages. The averaged spectrum was then processed for pre-edge subtraction and normalization using Cromer-Libermann calculations and for post-edge background subtraction using Ifeffit [51] algorithm to extract EXAFS signals. The processed data were imported into EXAFSPAK for coordination structure analysis. Structural information was determined by fitting the spectra with non-linear least-squares methods using phase and amplitude parameters obtained from theoretical calculation results of FEFF8 [52]. Fitting each shell results in the determination of the coordination number (CN) and the bonding distance (R) for the complex. The Debye-Waller factor, σ^2 , and ΔE_0 were allowed to vary during the optimization of CN and R. The excitation energy is converted into k-space, E_0 is defined as the energy at which the EXAFS spectrum begins and $k = 0$. The same ΔE_0 was used for all scattering paths within a single sample. Also the same σ^2 value was used

for each scattering pathway across multiple samples. The resulting CN and R, based on this fitting procedure, are expected to be accurate to $\pm 10\%$ and $\pm 0.02 \text{ \AA}$, respectively, for the first shell when single absorber-scatterer paths are used [53].

4.2 ESTIMATION OF TIME TO APPARENT EQUILIBRIUM

Cadmium adsorption rate experiments were conducted with the glycine, cysteine, and PLC electrodes using an initial cadmium concentration of approximately 5 mg/L. A higher initial concentration of 20 mg/L was used for the Ni experiment with the PLC electrode due to the weaker Ni-thiol binding constant. Figure 15 and Figure 16 show that between 50 and 90 percent of the metal ion is removed for all of the experiments except for the Cd-PLC system. For many adsorption systems involving macromolecules or porous adsorbents, evidence for a rapid adsorption step followed by a much slower approach to equilibrium has been observed [54, 55]. A sample taken after 150 min in the PLC-Ni experiment showed a concentration within 10% of the 60 minute concentration, suggesting that there may be a slow approach to true equilibrium. Each electrode shows a flattening of the concentration profile within approximately 30 min of equilibration time. As a result, 40 min was chosen as a suitable time between perturbation and measurement for adsorption edge and isotherm experiments. Therefore, the equilibrium concentrations reported after 40 min represents apparent equilibrium dominated by a rapid adsorption step.

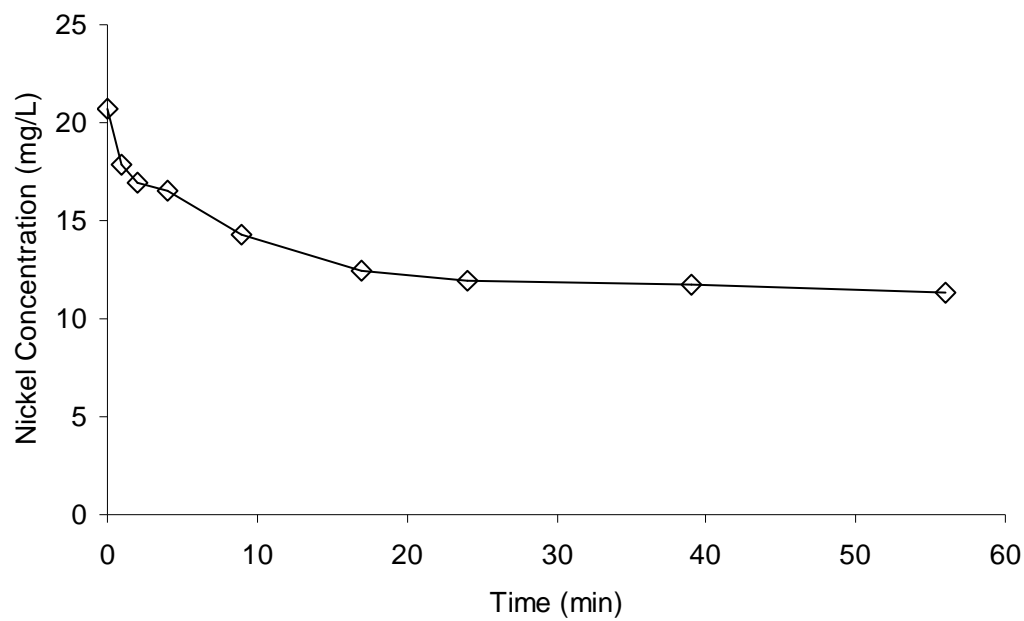


Figure 15. Nickel concentration in a batch kinetic test of adsorption onto a PLC electrode.

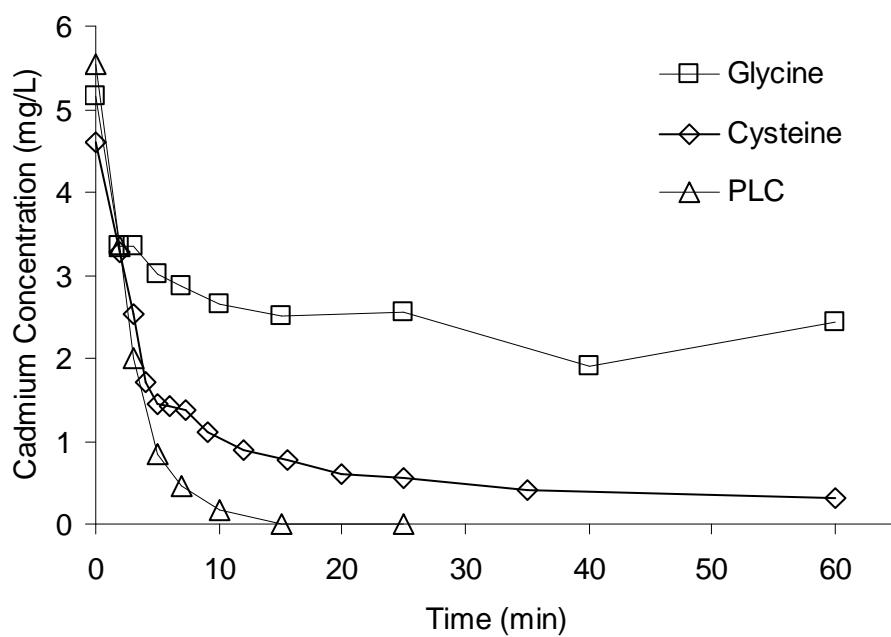


Figure 16. Cadmium concentration in a batch kinetic test of adsorption onto Gly, Cys, and PLC electrodes.

4.3 CADMIUM ADSORPTION RESULTS

The section presents results from cadmium adsorption edge, adsorption isotherm, and XAS experiments on metal loaded ESIE electrodes. Preliminary evaluations of the adsorption model are undertaken and the basis for refinement is established.

4.3.1 pH dependent adsorption behavior of Cd^{2+}

Oxidized and reduced electrodes were exposed to solutions containing ~1 mg total Cd^{2+} in 100 mL of total volume at low pH (<2). Step-wise increases in the pH of the recirculating solution resulted in typical adsorption behavior for surface complexation of metal ions in which protons are released as the metal ion adsorbs as shown in Figure 17. This behavior was evident for both the oxidized and reduced PLC-RVC. In addition, desorption edges obtained by step-wise reduction in pH did not exhibit hysteresis suggesting that the adsorption process is completely reversible within the time frame of these experiments.

A comparison of the reduced and oxidized edges shows differences in the extent of adsorption and a distinct pH behavior in each situation. The capacity of the reduced edge is greater for all pH values greater than 4. In addition, the pH to obtain 50% removal is approximately 6 for the oxidized edge, whereas 100 percent of the Cd^{2+} is removed on the reduced surface at the same pH. The steepness of the reduced PLC-RVC adsorption edge is representative of a strongly binding metal ion. A transition occurs from little adsorption at pH 3 to significant adsorption at pH 5. The oxidized edge shows very different behavior where adsorption increases steadily over 5 units of pH. This behavior is typical of a weakly binding cation. The differences between the adsorption behavior in these two systems suggests that the proton release and/or the structure of the surface complex has changed.

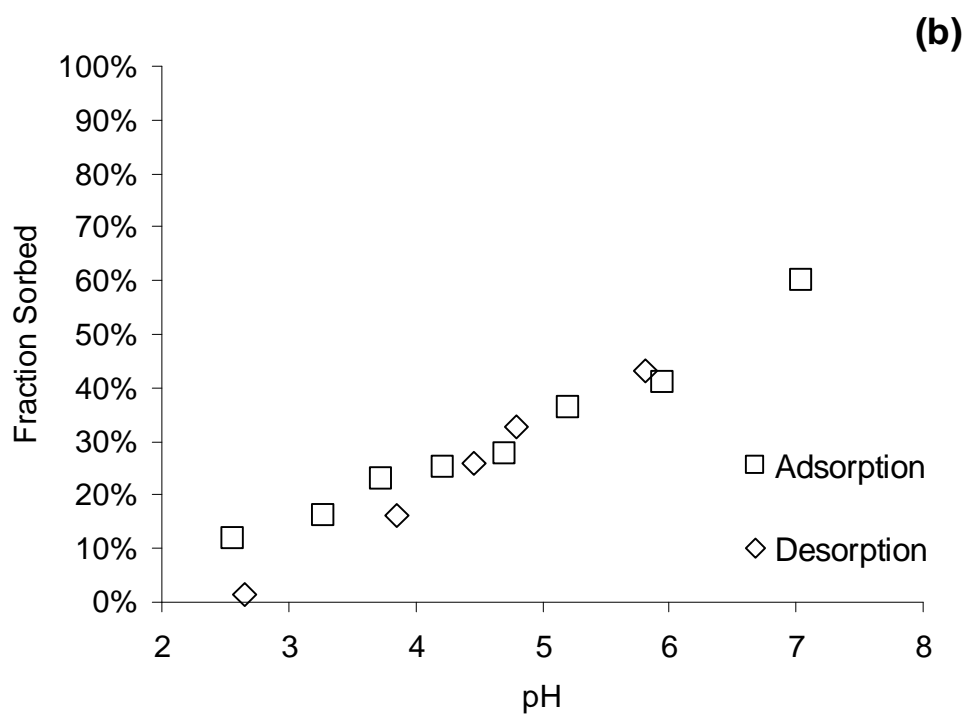
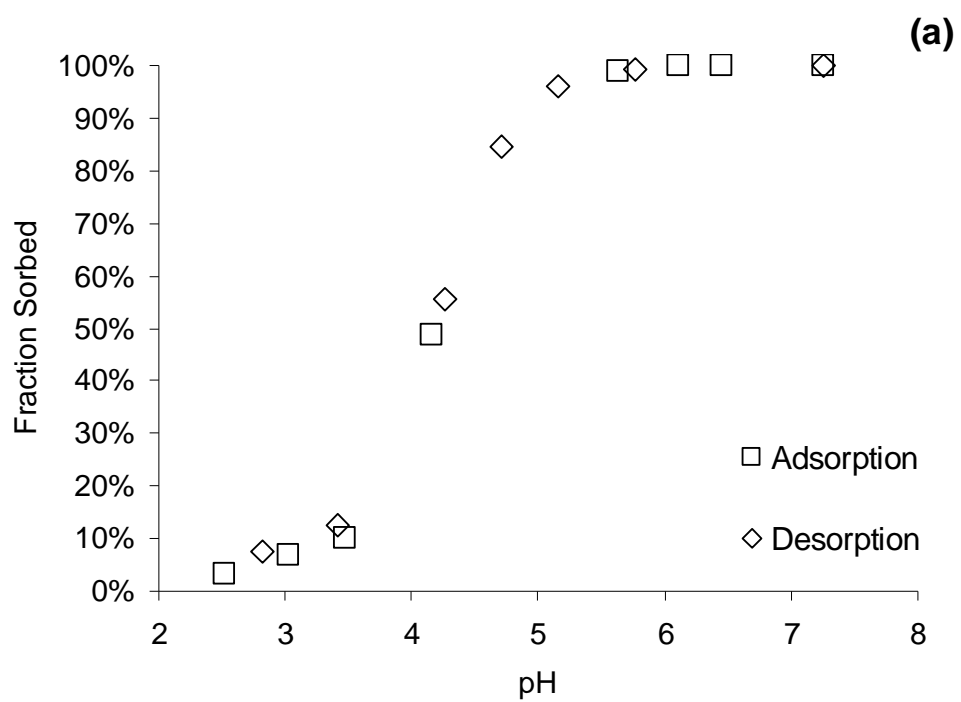


Figure 17. Cadmium adsorption/desorption edge on reduced (a) and oxidized (b) PLC-RVC (10 mg/L total metal concentration, 0.015 M ionic strength)

4.3.2 Cadmium Adsorption Isotherm Results

Several adsorption isotherm experiments were run on the PLC electrode to further characterize metal adsorption properties. Two important characteristics of the ESIE system that relate to the primary hypotheses of this research are shown experimentally:

- Redox reactions create distinct metal adsorption properties on the surface of the ESIE electrode
- Changes resulting from these redox reactions are reversible both chemically and electrochemically

Figure 18 compares Cd^{2+} adsorption isotherms developed at pH 7 with a PLC-RVC electrode that was reduced with DTT and the same electrode subsequently oxidized with H_2O_2 . The similarity between the isotherms developed from two experiments conducted with the oxidized electrode demonstrates the reproducibility of the data. The reduced electrode shows greater adsorption capacity relative to the oxidized electrode with a maximum capacity of approximately 10 mg/m^2 of Cd^{2+} adsorbed to the surface of a single electrode. In contrast, the oxidized electrode appears to be saturated with Cd^{2+} at 6 mg/m^2 . These data confirm the hypothesis that adsorption properties can be altered by changing the oxidation state of the substrate.

The same electrode used for the DTT reduced and H_2O_2 oxidized adsorption experiments was then subjected to over 10 redox cycles to demonstrate the reversibility of the ESIE process. Electrochemical reduction of an H_2O_2 oxidized electrode restored the adsorption capacity of the electrode to the same value as determined previously for the DTT reduced electrode as shown in Figure 19. Maximum adsorption again approached 10 mg/m^2 Cd^{2+} for a single electrode. Figure 19 also illustrates that a -0.8 V (vs Ag/AgCl) potential was sufficient to restore the capacity of the electrode.

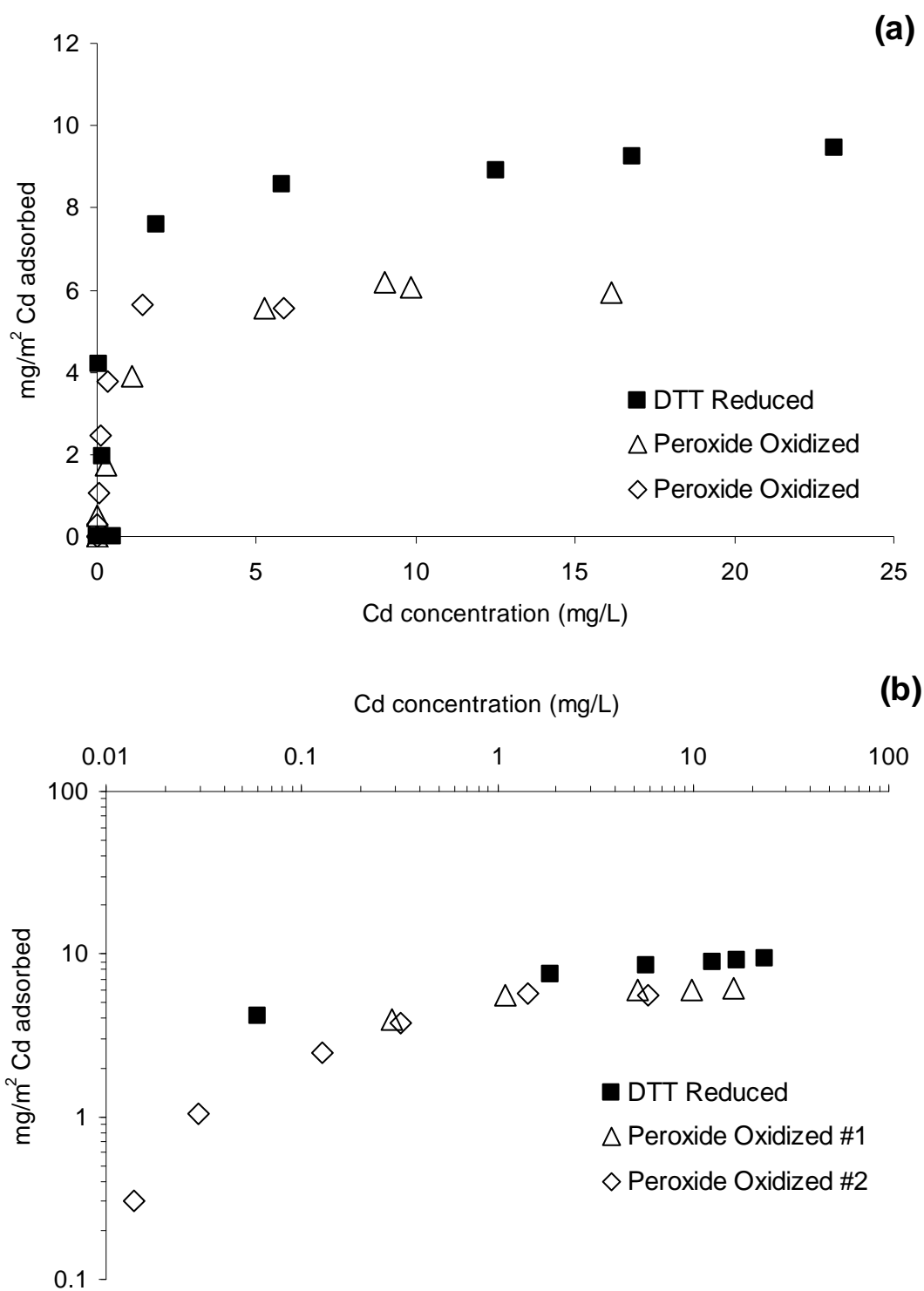


Figure 18. Cd^{2+} adsorption density onto DTT reduced and two H_2O_2 oxidized PLC-RVC electrodes. Normal scale (a) and log-log scale (b).

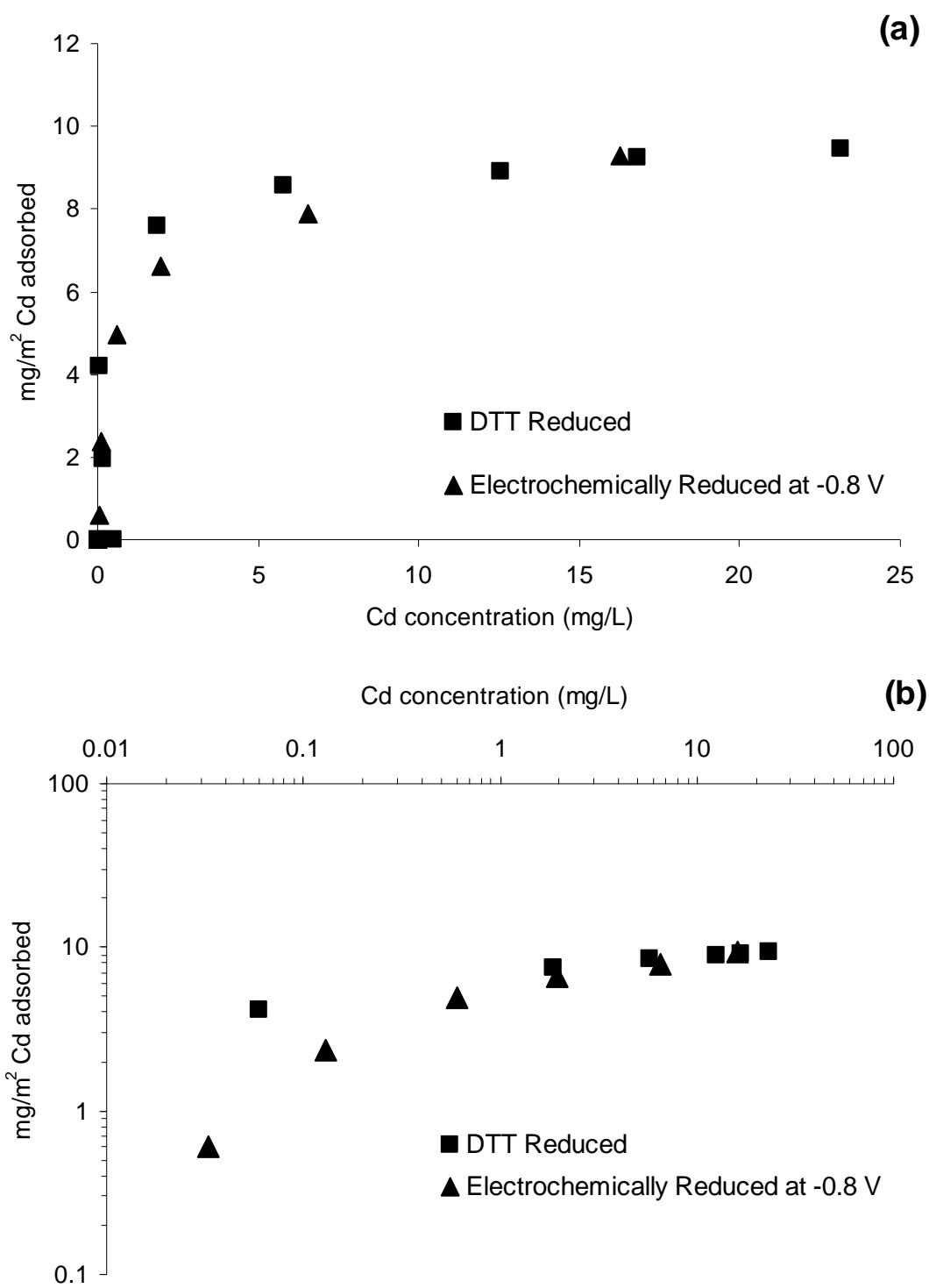


Figure 19. Cd²⁺ adsorption density onto DTT and electrochemically reduced PLC-RVC electrodes. Several redox cycles were performed between the two trials. Normal scale (a) and log-log scale (b).

Reduction of the electrode with NaBH₄ produced a change that was not completely reversible by either oxidation method. NaBH₄ is a much stronger reductant than DTT as shown by the significantly lower E° value presented in Table 6. The -0.8 V vs. Ag/AgCl potential applied to electrochemically reduce the surface is equivalent to -0.6 V vs. the standard hydrogen electrode (SHE) and represents an applied voltage that is intermediate between the two chemical reductants.

Table 6. Redox potentials of reagents

Redox Couple	E° (V)	Source
$\text{NaBH}_4 + 8 \text{OH}^- \leftrightarrow \text{NaH}_2\text{BO}_3 + 5 \text{H}_2\text{O} + 8 \text{e}^-$	-1.24	[56]
$\text{Cd}_2^+ + 2 \text{e}^- \leftrightarrow \text{Cd(s)}$	-0.403	[46]
DTT @ pH 8.1	-0.366	[3]
$\text{R-SS-R} + 2 \text{H}^+ + 2 \text{e}^- \leftrightarrow 2 \text{R-SH}$	-0.210	[3]
$\text{O}_2 + 4 \text{H}^+ + 2 \text{e}^- \leftrightarrow 2 \text{H}_2\text{O}$	+1.23	[46]
$\text{H}_2\text{O}_2 + 2 \text{H}^+ + 2 \text{e}^- \leftrightarrow 2 \text{H}_2\text{O}$	+1.78	[46]

The NaBH₄ reduction resulted in a permanent increase in capacity of the oxidized and reduced electrodes as shown in Figure 20. However, the relative increase in adsorption (3 mg/m²) was similar for both the reduced and oxidized electrode. Capacity on the NaBH₄ reduced electrode approached 14 mg/m² Cd²⁺ adsorbed on a single electrode, while the oxidized electrodes showed a lowered capacity of 10 mg/m² Cd²⁺. Previous experiments did not exceed 10 mg/m² of Cd²⁺ adsorbed for either surface oxidation state, so the NaBH₄ created an irreversible increase in capacity. A summary of the estimated capacity for each isotherm experiment is listed in Table 7.

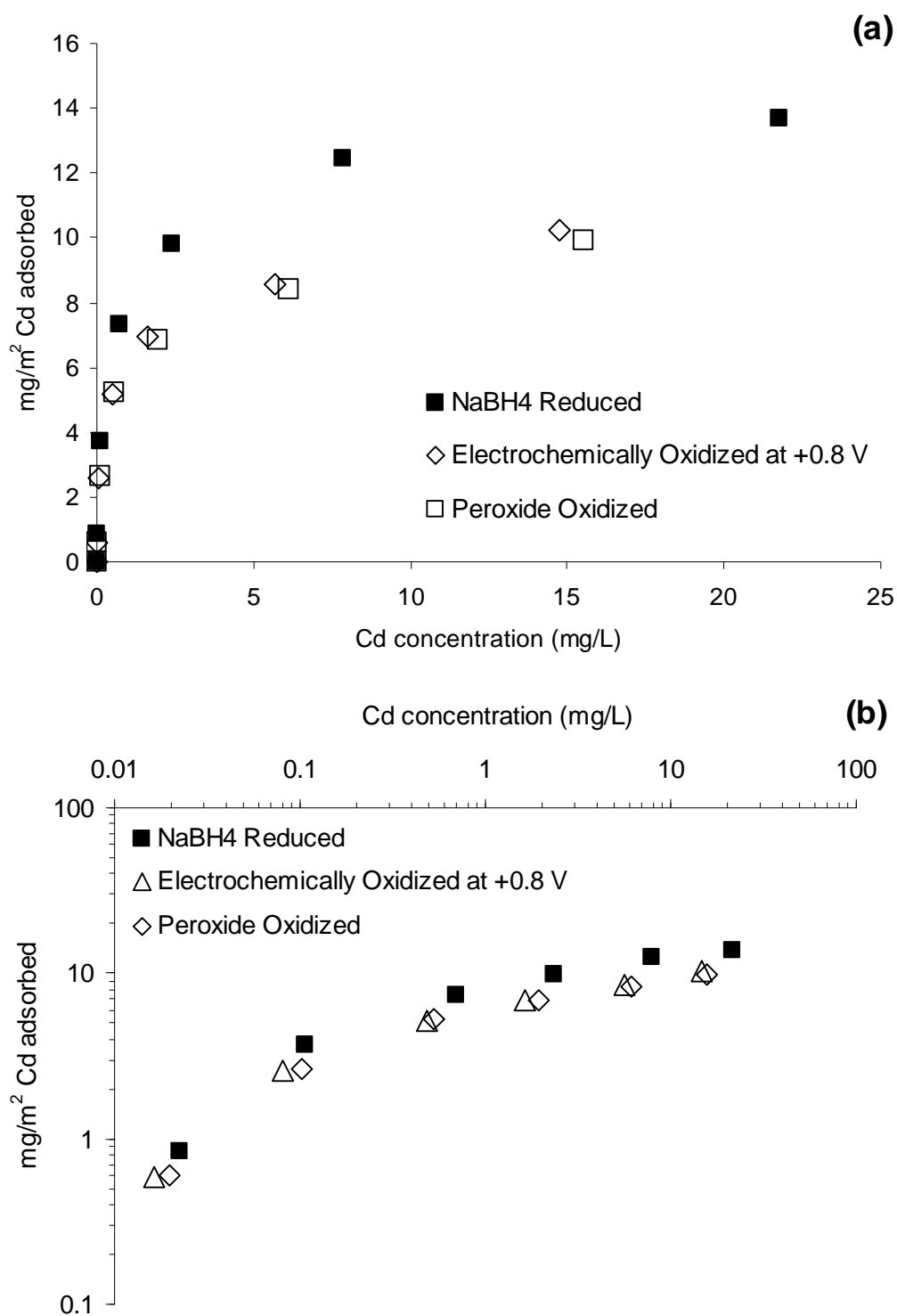


Figure 20. Cd²⁺ adsorption density onto a NaBH₄ modified PLC-RVC electrode. Initial reduction and electrochemical and H₂O₂ oxidations are compared. Normal scale (a) and log-log scale (b).

Table 7. Estimated Cadmium Capacity for PLC-RVC Isotherm Experiments

Electrode	Redox State	Redox Agent	Estimated Cd ²⁺ Capacity (mg/m ²)
PLC-RVC	Reduced	DTT	10
PLC-RVC	Reduced	Potential	10
PLC-RVC	Oxidized	H2O2	6
PLC-RVC-NaBH ₄	Reduced	NaBH ₄	13
PLC-RVC-NaBH ₄	Oxidized	Potential	10
PLC-RVC-NaBH ₄	Oxidized	H2O2	10

Table 7 shows that capacities for each electrode are greater in the reduced state than the oxidized state by approximately 3 mg/m² of Cd²⁺. All electrodes retain significant capacity in the oxidized state. The basis of the switching in the ESIE system is the proposed oxidation of cysteines. Each oxidized cysteine is effectively the loss of a site for metal binding. The reduction in capacity confirms that the imposed voltage affects the surface of the electrode and cysteine oxidation is the most reasonable mechanism for the lowered capacity. Cysteine thiols oxidize to disulfides if two thiols are sterically available to each other. Under strong oxidizing conditions such as H₂O₂, if a second thiol is not available for reaction, sulfonates can form, which would also reduce metal binding capacity [57, 58]. Others have found similar results with PLC on different substrates [3], and this work expands on existing work with application of electrochemical oxidation at lab scale. An examination of the redox potentials of the redox agents used in Table 6 support this assessment. The thiol/disulfide couple has a standard reduction potential of -0.210 V vs. SHE. The redox couples that have lower standard reduction potentials and reduce disulfides to thiols and the couples that have higher potentials and oxidize disulfides to thiols are shown in Table 6. The

electrochemical potentials of -0.8 V and +0.8 V vs Ag/AgCl applied in this system correspond to approximately -0.6 V and +1 V vs SHE.

The capacity of the oxidized electrode can be attributed to thiols which cannot form disulfide bonds due to steric limitations, the carboxylate present at the C-terminus of the PLC peptide, and unreacted carboxylate functional groups present on the surface of the carbon electrode. These groups are not readily reduced by either DTT or the electrochemical reduction applied to the surface. Additionally, NaBH₄ is not a strong enough reducing agent to reduce carboxylic acids [59].

The increase in capacity seen following NaBH₄ reduction did not significantly contribute to the switchable metal capacity of the system. The difference between reduced and oxidized conditions remained approximately 3 mg/m² for a single electrode. It is possible that NaBH₄ reduced thiols that were not able to be re-oxidized by the methods used in this research. Also, NaBH₄ could reduce other carbon-oxygen functionalities such as aldehydes or thiol esters which would provide more capacity that could not be re-oxidized [59].

Initial analysis of the reduced and oxidized isotherms has established the ability to increase and decrease metal binding capacity by reducing or oxidizing the electrode, respectively. This change can be performed chemically or electrochemically with similar results in each case. Capacities estimated for the reduced and oxidized states can be used with adsorption edge data to refine the adsorption model for the ESIE system.

4.3.3 Cadmium PLC-RVC XAS Analysis and Results

This study focused on identifying the coordination environment of cadmium adsorbed on the surface of the ESIE electrode. Specifically differences between the cadmium environment in the reduced and oxidized states of the ESIE system were examined.

Cd K-edge XANES spectra collected for the two ESIE samples showed no significant differences as seen in Figure 21. It was expected that different Cd-O or Cd-S coordination would affect the corresponding XANES spectrum and therefore serve as an indicator of change of coordination environment. While it is true in general that XANES is sensitive to geometric structural change of nearest neighboring atoms, Cd K-edge XANES has some properties that affect interpretation of the spectra for this work. Cd K-edge has a relatively short core-hole lifetime, and this short lifetime broadens the K-edge XANES spectrum. This broadening effect masks the different features originated from Cd-O and Cd-S coordination structure [60]. Indeed, Cd L_I or L_{III}-edge XANES spectra are more appropriate for analyzing Cd-O and Cd-S coordination because of their lack of broadening effect and sensitivity to detailed cadmium local structure [61]. Unfortunately, due to limited beam time available to this study, Cd L-edge XANES spectra were not collected. Nevertheless, EXAFS analysis provides definitive results for the coordination environment of Cd²⁺ as discussed below.

To provide a baseline for discussion of the EXAFS data collected in this research, literature pertaining to EXAFS analysis of cadmium-sulfur interactions was reviewed. Studies of Cd-S interactions through EXAFS have been reported in the context of cadmium complexation with cysteine containing clays [62], cadmium coordinated proteins [60, 63], cadmium-thiol interactions in natural organic matter [64, 65], thiol compounds in solution [66], and on cadmium sulfide nanoparticles [61]. Cadmium has distinct coordination structures for oxygen (octahedral) and sulfur (tetrahedral). In aqueous solution, cadmium is coordinated by the oxygens of six water molecules, and sulfur coordination generally consists of four sulfur atoms [66]. A consistent bonding distance (R) of 2.43 to 2.54 Å appears for the primary Cd-S interaction in all of the literature cited. Many of the same studies also found that primary Cd-O interactions have

shorter bond distances of 2.16 to 2.27 Å. The ESIE system contains thiols as functional group on cysteines, and also contains oxygen functionalities as carboxylic acids at the terminus of the PLC peptide, on the surface of the carbon electrode, and in the peptide backbone. Additionally, the oxygen present in water coordinates free cadmium in solution. These conditions lead to the expectation that both oxygen and sulfur interactions would be seen in the ESIE system as in several of the systems cited above.

EXAFS spectra and corresponding Fourier transforms are shown in Figure 22 for the reduced state and Figure 23 for the oxidized state. Parameters extracted from EXAFS fitting are shown in Table 8.

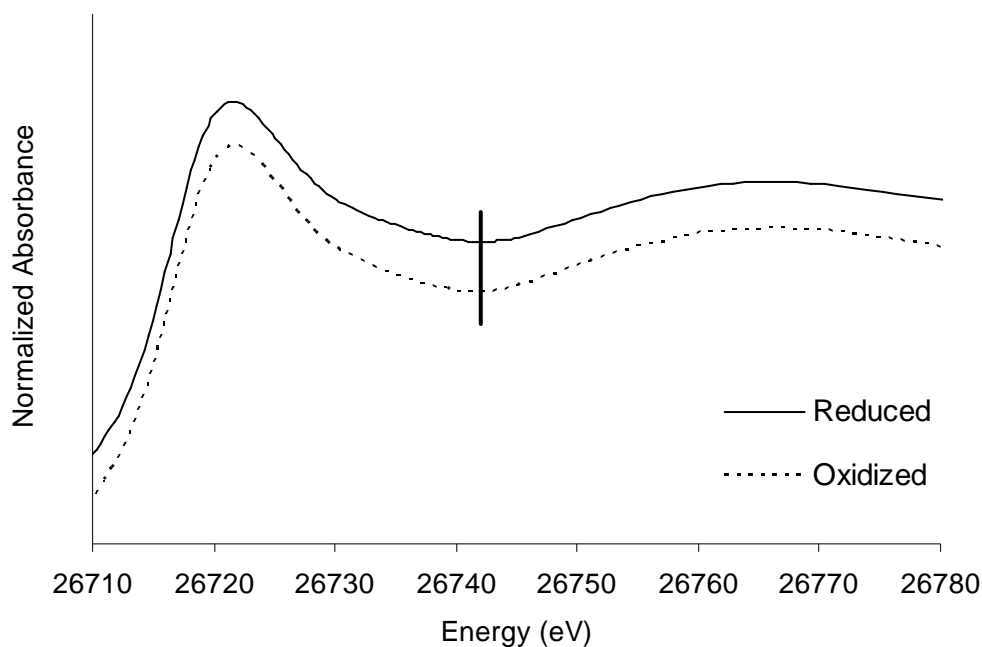


Figure 21. XANES Spectra for Cd^{2+} on reduced and oxidized PLC-RVC. The vertical line represents a minimum in the absorption spectra of both samples.

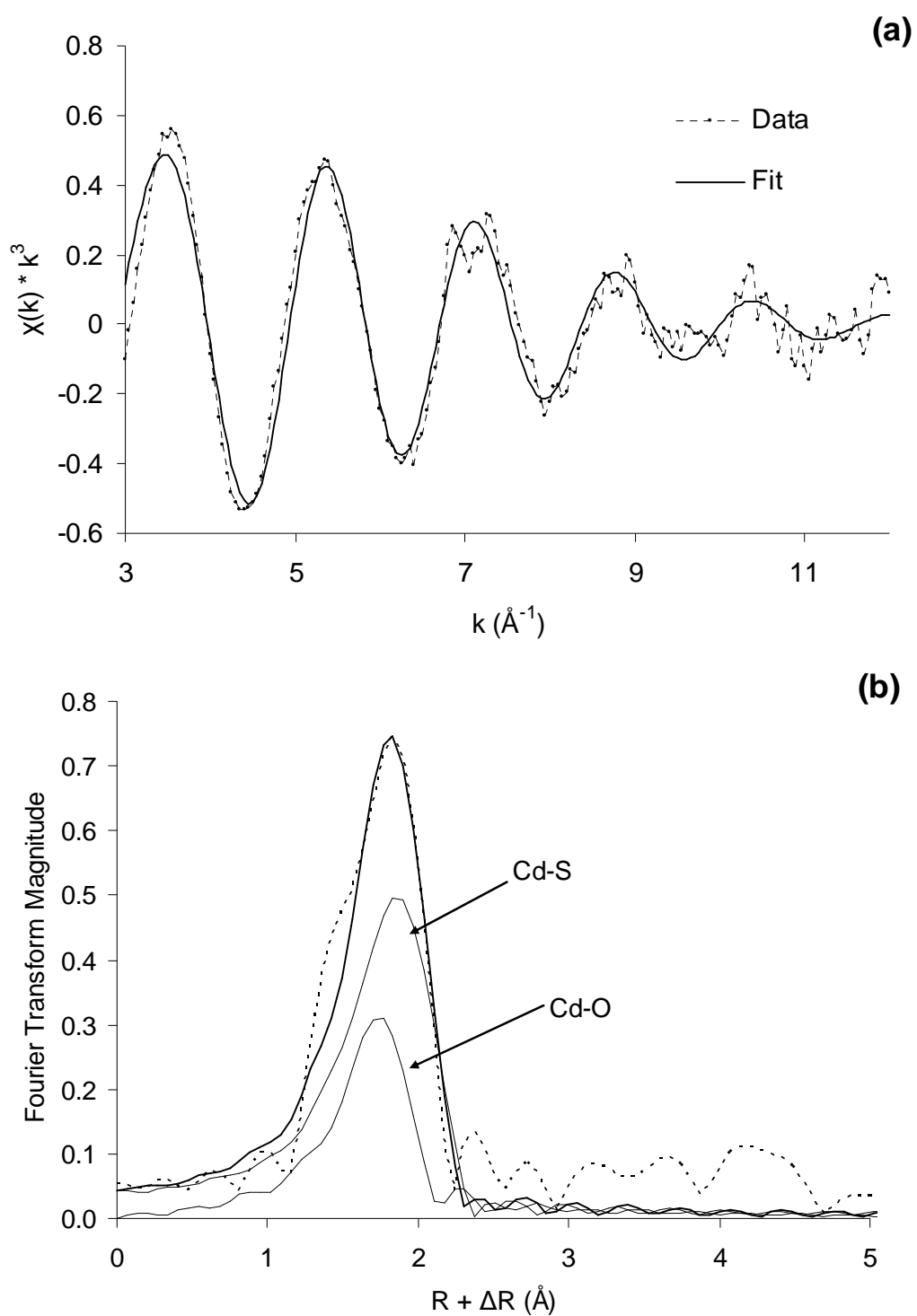


Figure 22. (a) EXAFS Spectra of Cd^{2+} on reduced PLC-RVC and (b) Fourier Transformed EXAFS Spectra of Cd^{2+} on reduced PLC-RVC. Dashed lines are data and solid lines represent the components of the fit and the total fit.

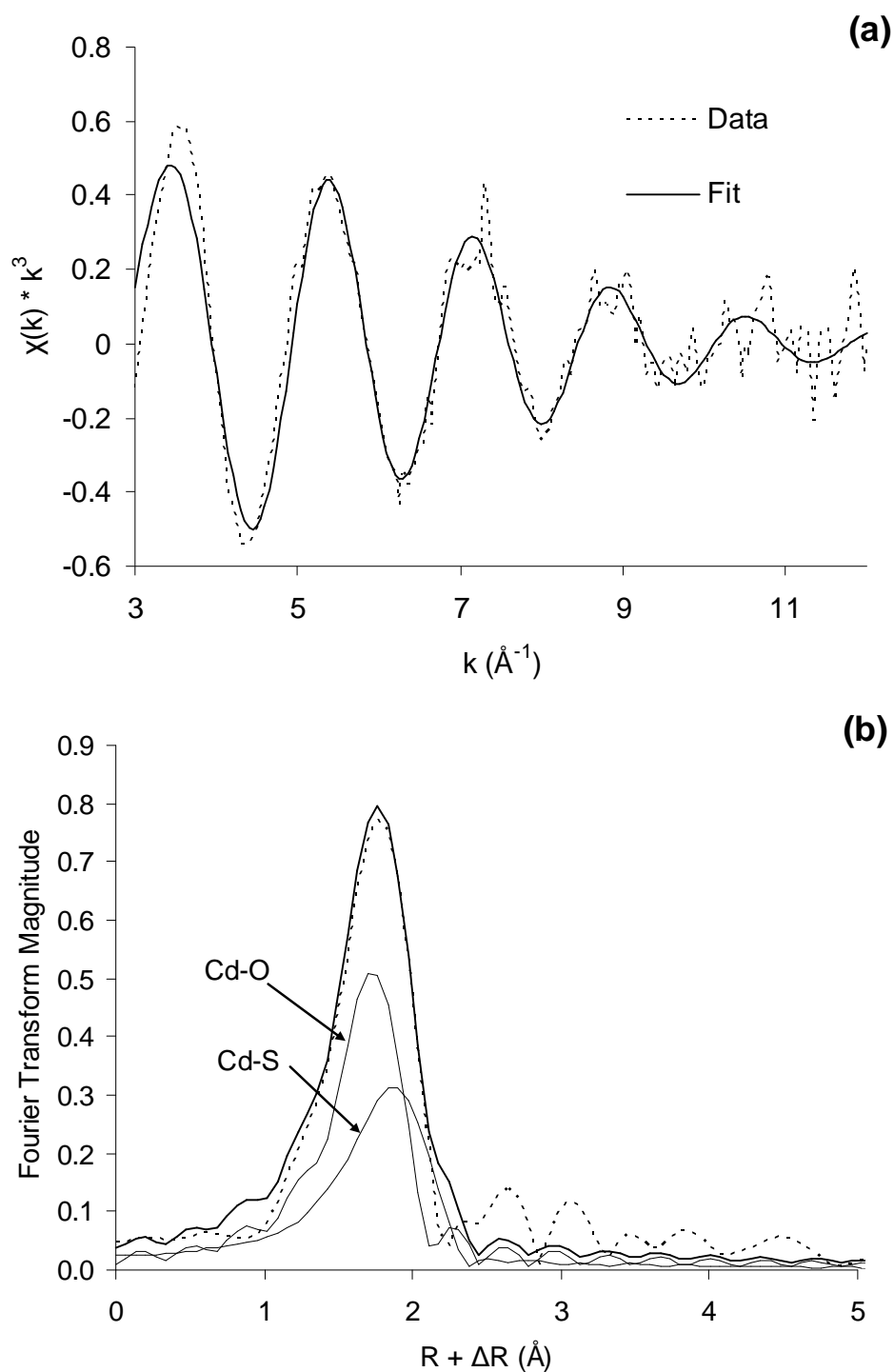


Figure 23. (a) EXAFS Spectra of Cd^{2+} on oxidized PLC-RVC and (b) Fourier Transformed EXAFS Spectra of Cd^{2+} on oxidized PLC-RVC. Dashed lines are data and solid lines represent the components of the fit and the total fit.

Table 8. EXAFS Parameters

	Cd-S			Cd-O			ΔE_0
	N	R (Å)	σ^2 (Å ²)	N	R (Å)	σ^2 (Å ²)	
Reduced	3.5	2.44	0.01360	1.9	2.27	0.00682	-14.5
Oxidized	2.2	2.44	0.01378	2.8	2.26	0.00629	-12.5

Interatomic distances (R) between cadmium and both sulfur and oxygen were within the range of previously mentioned literature values for both the oxidized and reduced electrode. Furthermore, the R values for Cd-S and Cd-O were the same within the precision of the fit (± 0.02 Å) for both the oxidized and reduced states. The value of R implies the strength of an interaction. A typical example in metal sorption to solid surfaces is a comparison of inner sphere and outer sphere coordination. Inner sphere interactions have shorter bonding distances since the metal and complexing atoms are in closer proximity. Outer sphere interactions often have waters of hydration between the metal and complexing atom. The presence of the water molecules increases the bonding distance and decreases the strength of the interaction. A powerful aspect of XAS is the ability to differentiate between these two scenarios [53]. Similar bonding distances for the oxidized and reduced states imply that the strength of the interaction between a cadmium atom and a single complexing sulfur is also the same. The bonding distance also implies an inner sphere interaction. Outer sphere interactions generally have bonding distances of 5 Å or greater [53].

Though the strength of each Cd-S/Cd-O interaction is the same in the oxidized and reduced states, the number of these interactions is distinct each case. The average coordination number (N) for the Cd-S interaction increases from 2.2 in the oxidized state to 3.5 in the reduced state. This implies that a greater number of sulfur atoms are

associated with each cadmium atom in the reduced state than in the oxidized state. Accordingly there is a decrease in the average oxygen coordination number when the electrode is reduced of 2.9 to 1.9. The assessment agrees with the hypothesis that there are more free thiols in the reduced state and the isotherm results.

A previous aqueous based EXAFS study of complexation of Cd^{2+} in solution by thiol compounds also found similar results with respect to coordination numbers [66]. Three thiol containing compounds, 2-mercaptoethylamine (MPEA), 2-mercaptoethylsulfonate (MPES) and 3-mercaptopropionic acid (MPA) were varied in concentration while metal concentration was fixed. The coordination of Cd^{2+} was compared by EXAFS analysis. Figure 24 is reproduced from that study. Thiol coordination increases with increasing thiol concentration up to a maximum of 4 thiols per Cd^{2+} (tetrahedrally coordinated). Oxygen coordination decreases as thiol concentration increases since thiols form a stronger complex and can displace oxygen complexes.

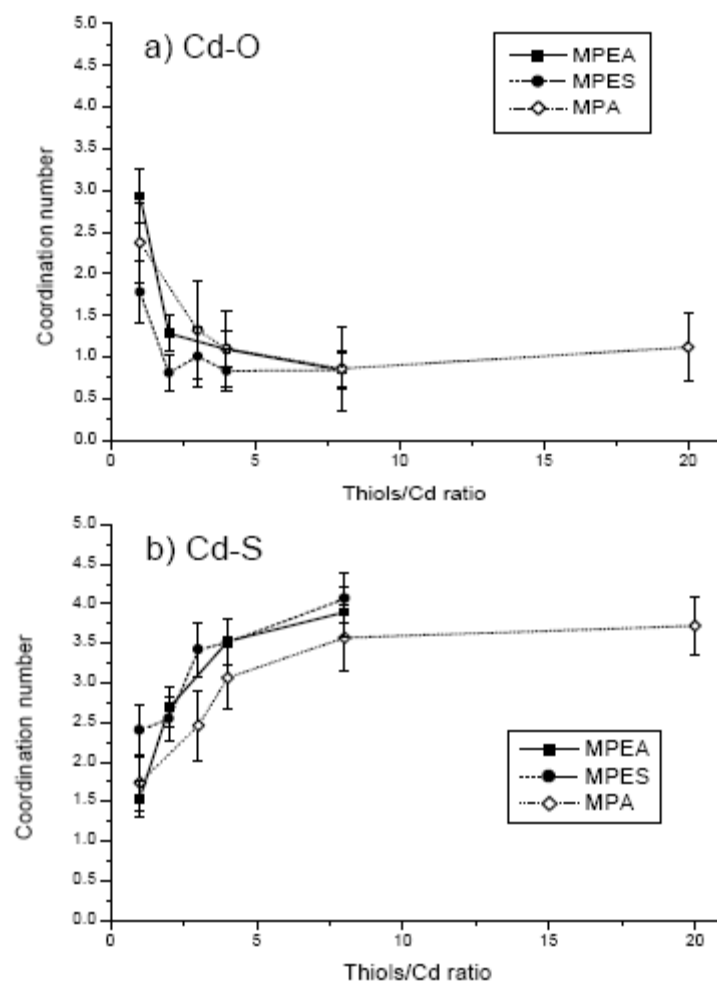


Figure 24. Coordination numbers of Cd-O (a) and Cd-S (b) bonds. (Reprinted with permission from IUCr) [66].

The ESIE system is comparable to this aqueous speciation based example, since the concentration of available thiols on the reduced surface is higher than in the oxidized state. A greater concentration of thiols on the surface would produce the same effect on speciation – a shift from oxygen coordination to sulfur coordination for cadmium over the surface of the electrode. The confirmation that multiple thiols associate with a single cadmium atom necessitates a change in the adsorption model.

4.4 CADMIUM ADSORPTION MODEL DEVELOPMENT

4.4.1 Baseline Model

This section establishes the foundation for a model of the pH dependent behavior of metal adsorption. This model will be evaluated and refined based on experimental results in the following sections. The simplified ion exchange model presented in Eqns. 2.1-2.4 does not account for proton-site interactions. The primary site for Cd^{2+} adsorption in the ESIE system is a thiol group. The protonation state of the thiol group is likely to have an effect on the complexation of a metal ion. Previous work by Jurbergs and Holcombe has established the pH dependence of Cd^{2+} adsorption on PLC as shown in Figure 25.

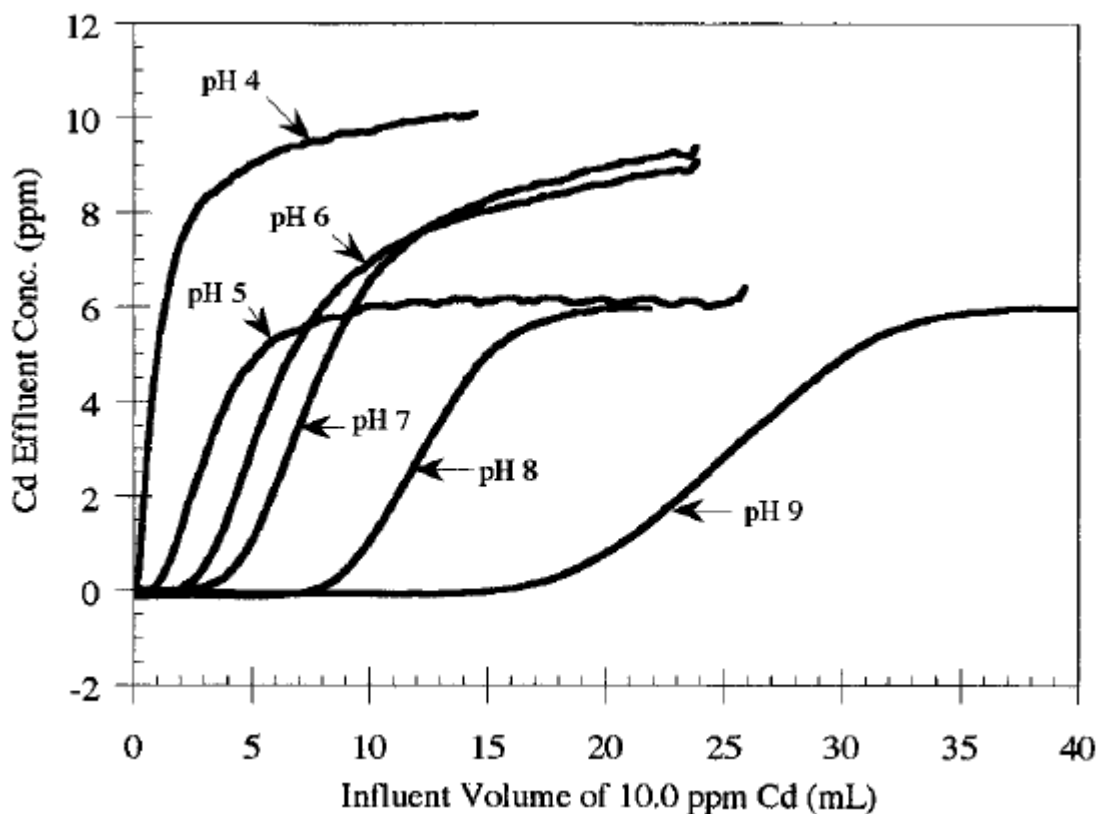
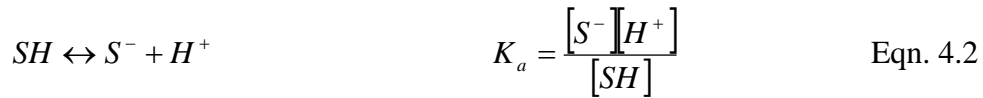
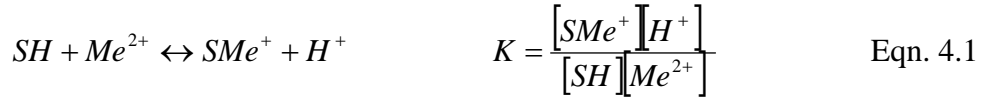


Figure 25. Breakthrough curves for Cd^{2+} adsorbing to reduced PLC immobilized on controlled pore glass. Influent concentration = 10 mg/L Cd^{2+} [4]

The breakthrough curves shown in Figure 25 shift to higher throughput volume with increasing pH. This observation is consistent with the generalized trend of increased cation adsorption with increasing pH that was evident in the sorption edges presented in and Figure 17. The interaction of protons with surface sites can be included in the existing site limited model of adsorption by adding a proton to both sides of Eqn 2.1 as shown in Stumm and Morgan [67]. The inclusion of a site protonation reaction gives Eqns. 4.1 through 4.4.



If the total number of sites is assumed to be a constant, then a mole balance can be added, and equations can be rearranged to give the concentration of occupied sites as a function of metal concentration and pH.

$$S_{TOT} = [SMe^+] + [SH] + [S^-] \quad \text{Eqn. 4.3}$$

$$[SMe^+] = \frac{S_{TOT} K [Me^{2+}]/[H^+]}{1 + K [Me^{2+}]/[H^+]} \quad \text{Eqn. 4.4}$$

This model predicts a change in adsorption when the proton concentration is on the same order of magnitude as the product of the adsorption equilibrium constant (K) and the free metal concentration. Little or no sorption is predicted for conditions where $K[Me^{2+}] \ll [H^+]$, maximum adsorption is predicted where $K[Me^{2+}] \gg [H^+]$ and the

transition between these two regions takes place over one to two orders of magnitude of pH in a manner similar to acid base speciation. These trends are apparent for the adsorption edges for Cd^{2+} in the reduced state. For an adsorption edge experiment the initial metal ion concentration is fixed and pH is varied. A mass balance on total metal can be added (Eqn. 4.5) to give all other concentrations as a function of pH.

$$Me_{TOT} = [SMe^+] + [Me^{2+}] \quad \text{Eqn. 4.5}$$

Once the metal concentration is known, adsorption can be represented as fraction of total metal in the system (Eqn 4.6).

$$\%ads = \frac{[SMe^+]}{Me_{TOT}} \quad \text{Eqn. 4.6}$$

Figure 26 shows the predicted percent adsorbed for a total metal concentration of 1×10^{-4} M metal, 2×10^{-4} M sites, K of 0.05, and K_a for surface sites of 1×10^{-10} M. This behavior is common among metal cations adsorbed to surfaces [67]. The slope of this curve is a function of the coefficient on the proton in Eqn. 4.1 as well as the initial solute concentration. The location of the edge is dependent on the initial solute and sorbent concentration as well as the value of the equilibrium constant for Eqn. 4.1.

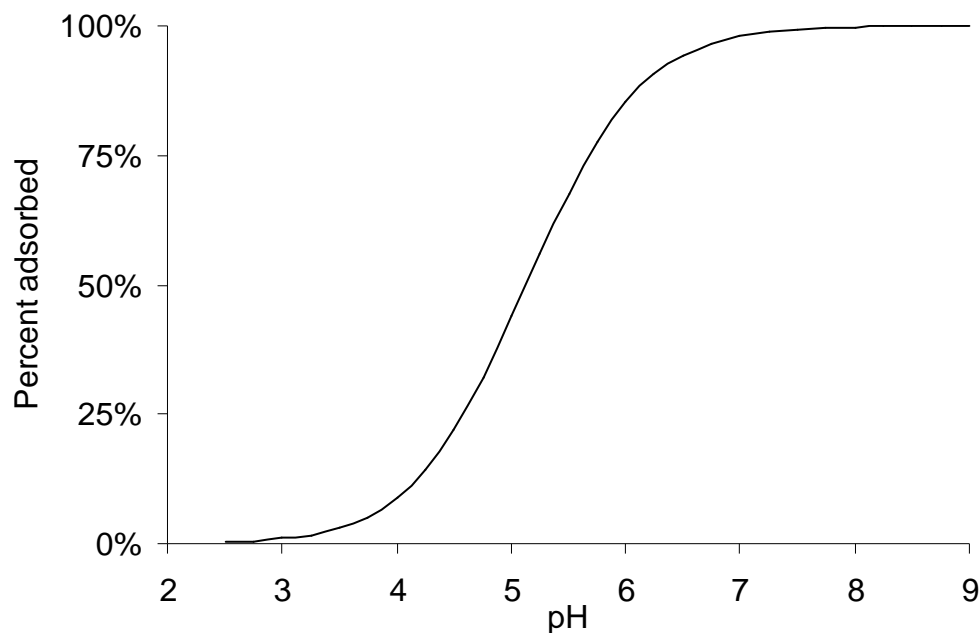


Figure 26. pH dependent site-limited model prediction of metal adsorption ($Me_{TOT} = 1 \times 10^{-4} \text{ M}$, $S_{TOT} = 2 \times 10^{-4} \text{ M}$, $K = 0.05$, $K_a = 1 \times 10^{-10} \text{ M}$)

The pH modified site-limited model does not contain the complexity necessary to represent both the oxidized and reduced edges presented in and Figure 17 because of the difference in pH behavior. The parameters available in the baseline model are the total number of sites, S_{TOT} , and the equilibrium constant for the adsorption reaction, K . The stoichiometry of the reaction forces a small range of reasonable values on the value of S_{TOT} . The maximum quantity of metal that can be adsorbed can be estimated from isotherm experiments presented in Section 4.3, and the assumption that each metal is adsorbed to a single site. The K_a for the site was taken from the value for cysteine, $10^{-8.2}$, though this value may be slightly lower for PLC [6]. This leaves K as the only variable parameter, and preliminary attempts to fit both the oxidized and reduced adsorption edge under these constraints are shown in Figure 28. A best fit K was estimated by minimizing the absolute square error between the percent adsorption for the predicted

edge and the experimental data. An outline of calculations performed are included in the appendix. The resulting parameters are shown in Table 9.

Table 9. Best fit parameters for the baseline model

	K	S_{tot} (M)	Sq. Error
Reduced	1.5	9.8×10^{-5}	0.108
Oxidized	0.49	5.4×10^{-5}	0.079

Though the reduced isotherm had a maximum adsorption of 10 mg/m^2 at pH 7, the S_{TOT} of the reduced edge in the model was increased to $11.6 \text{ mg/m}^2 \text{ Cd}^{2+}$ to account for slight disagreement between the edge and isotherm in order to obtain a satisfactory fit. The reduced edge showed 100% adsorption at high pH values and the total metal initially added to the experiment was 11.6 mg/m^2 of Cd^{2+} , so it followed that there must be at least that many sites in that experiment.

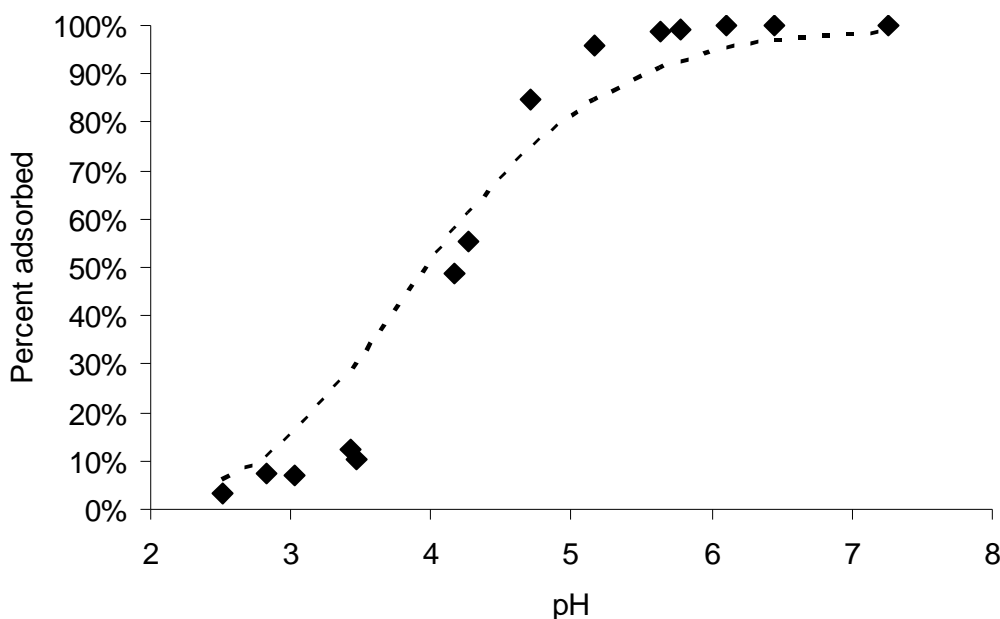


Figure 27. Baseline model fit for Cd^{2+} on reduced PLC-RVC. $K = 1.5$, $S_{\text{tot}} = 9.8 \times 10^{-5} \text{ M}$

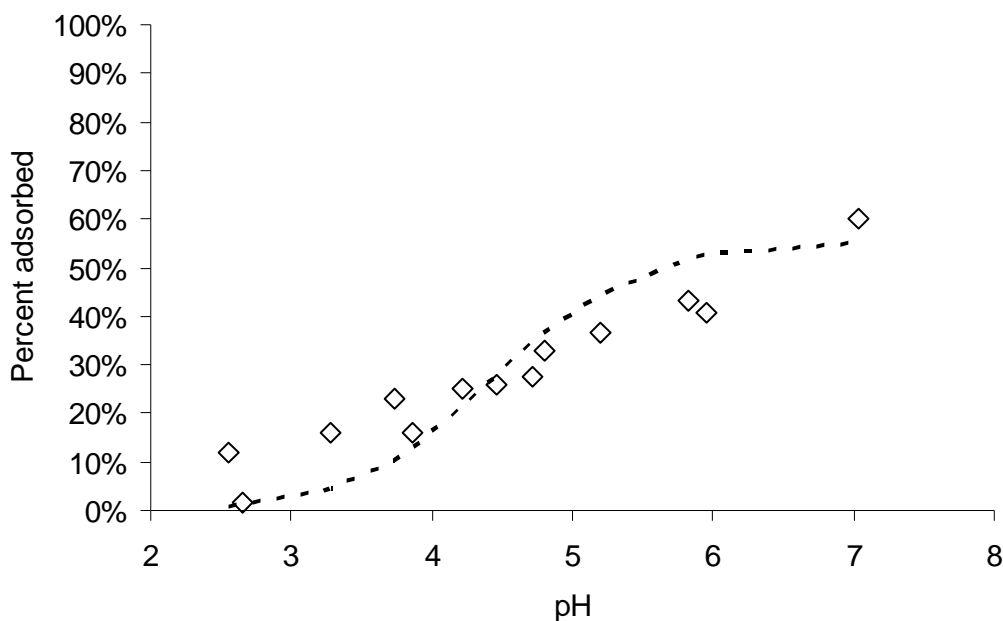


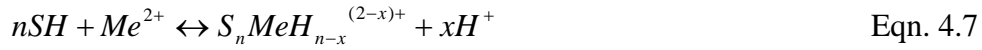
Figure 28. Baseline model fit for Cd^{2+} on oxidized PLC-RVC. $K = 0.49$, $S_{\text{tot}} = 5.4 \times 10^{-5} \text{ M}$

The model fit of adsorption on the reduced electrode was not steep enough to capture the total adsorption at high pH and overestimated adsorption at low pH. The model fit to the adsorption data for the oxidized electrode using the same binding constant (K) but a reduced site density was too steep to match the experimental data. To fit the data for this electrode, it was necessary to reduce the binding constant by a factor of three and the total site density by a factor of approximately two. Even with these modifications, the model overpredicted most of the sorption data at high pH and underpredicted sorption at low pH. Thus, the baseline model poorly predicted the pH behavior of both oxidized and reduced adsorption edges. Additional complexity is necessary to describe the pH dependent behavior of the oxidized and reduced electrode. Insights gained from spectroscopic data and reinforced by literature provide a rationale to modify the baseline model.

4.4.2 Multidentate model for Cd^{2+} sorption

A single site-single metal interaction model does not fully capture the complexity of the adsorption edge experimental results. The slope of the transition region of the edge is not properly characterized by the baseline model. Incorrect stoichiometry in the model could explain the inability to correctly model the slope. A rationale for changing the stoichiometry of the adsorption reaction is presented in this section.

Coordination numbers derived from EXAFS imply multiple sulfurs interacting per cadmium. The EXAFS data for the reduced PLC-RVC electrode showed average Cd^{2+} coordination of 3.5 sulfurs per cadmium and the oxidized PLC electrode showed average sulfur coordination of 2.2 sulfurs per cadmium. Previous studies of PLC-cadmium binding also find multiple thiols per cadmium [4]. Multiple sulfurs complexing a single cadmium could release multiple protons. A change in proton stoichiometry has a direct effect on the slope of the adsorption edge. A generalized n site model for cadmium surface complexation and x protons released is shown below.



$$K = \frac{[S_n\text{MeH}_{n-x}^{(2-x)+}][H^+]^x}{[SH]^n[\text{Me}^{2+}]} \quad \text{units } \text{M}^{x-n} \quad \text{Eqn. 4.8}$$



$$K_a = \frac{[S^-][H^+]}{[SH]} \quad \text{Eqn. 4.10}$$

$$S_{TOT} = n[S_n\text{MeH}_{n-x}^{(2-x)+}] + [SH] + [S^-] \quad \text{Eqn. 4.11}$$

$$Me_{TOT} = \left[S_n MeH_{n-x}^{(2-x)+} \right] + \left[Me^{2+} \right] \quad \text{Eqn. 4.12}$$

This includes two additional parameters to the model – the number of sites coordinating per cadmium and the number of protons released per cadmium adsorbed. The coordination numbers estimated from EXAFS analysis suggest that the reduced PLC has 3.5 sulfurs per cadmium and the oxidized PLC has 2.2 sulfurs per cadmium. Since EXAFS is an averaging technique, the non-integer values indicate that multiple coordination numbers are possible. However, for simplicity only a single whole number was used for the value of n. Multiple values for n necessitate multiple reactions with different stoichiometries and binding constants. More experimental data under a wider array of conditions are required to differentiate multiple reactions.

Using the EXAFS coordination values as a guideline, the adsorption edge for the reduced electrode was fit with $n = 3$ and $n = 4$, and the oxidized model incorporated values of $n = 3$ and $n = 2$. All values of k less than or equal to n were tested for each n. As with the baseline model, the range of reasonable values of S_{TOT} is determined by results from the isotherm experiments. Again an adjustment to increase S_{TOT} was made to account for disagreement between the reduced isotherm and edge. Since each metal in this model takes n sites the value of S_{TOT} must correspond to n times the maximum metal concentration. A summary of the sources for each parameter are listed in Table 10.

Table 10. Multidentate model parameters

Parameter	Source
S_{TOT}	Isotherm/Edge maximum adsorption
n	Estimation from EXAFS coordination
x	Assumption that $x \leq n$
K_a	Literature value for cysteine
K	Fitted parameter

Eqn 4.8 and Eqns. 4.10-4.12 were solved for a given pH to give metal concentration which was then converted to fraction adsorbed. The model predicted fraction adsorbed was calculated at the same pH as each data point. The square absolute error between the model prediction and the data was summed and minimized by varying K . Square absolute error was chosen as it weights the transition area of the edge more than the high and low adsorption areas. Changes in percent adsorption with respect to pH are small at both ends of the edge. Further evaluation of the fits was carried out by examining the fit of the log of the free metal concentration for the data and the fits with the least error. Additional description of the model calculations is included in the appendix. This was repeated for each combination of n and x . The minimum square error for each $n/x/K$ combination was tabulated and is shown in Table 11. Plots for the two best reduced fits are shown in Figure 29 and the two best oxidized fits are shown in Figure 30.

Table 11. Best fit parameters for the multidentate model

	n	x	K (M^{X-N})	S _{tot} (M)	Square Error
Reduced	1	1	1.5	9.82×10^5	0.1078
Reduced	3	2	2000	2.95×10^4	0.0627
Reduced	3	1	2.30×10^7	2.95×10^4	0.4366
<i>Reduced</i>	<i>4</i>	<i>4</i>	<i>0.021</i>	<i>3.93×10^4</i>	<i>0.0339</i>
<i>Reduced</i>	<i>4</i>	<i>3</i>	<i>390</i>	<i>3.93×10^4</i>	<i>0.0341</i>
Reduced	4	2	4.30×10^6	3.93×10^4	0.1194
Reduced	4	1	5.10×10^{10}	3.93×10^4	0.6202
Oxidized	1	1	0.49	5.36×10^5	0.0792
Oxidized	2	2	0.19	1.07×10^4	0.1361
<i>Oxidized</i>	<i>2</i>	<i>1</i>	<i>5600</i>	<i>1.07×10^4</i>	<i>0.0423</i>
Oxidized	3	3	0.038	1.61×10^4	0.1640
Oxidized	3	2	1500	1.61×10^4	0.0980
<i>Oxidized</i>	<i>3</i>	<i>1</i>	<i>3.20×10^7</i>	<i>1.61×10^4</i>	<i>0.0347</i>

Examination of Figure 29 illustrates that increasing the value of n, increases the slope of the predicted edge in the transition region. The baseline model underpredicted adsorption at high pH and overpredicted at low pH because of the inability to capture the slope of the experimental data. The multidentate model allows flexibility in the slope through the n and x parameters which are exponents in the characteristic equilibrium expression shown in eqn. 4-10. The slope can also be increased by increasing the value of k as shown in the difference between the two plotted parameter sets.

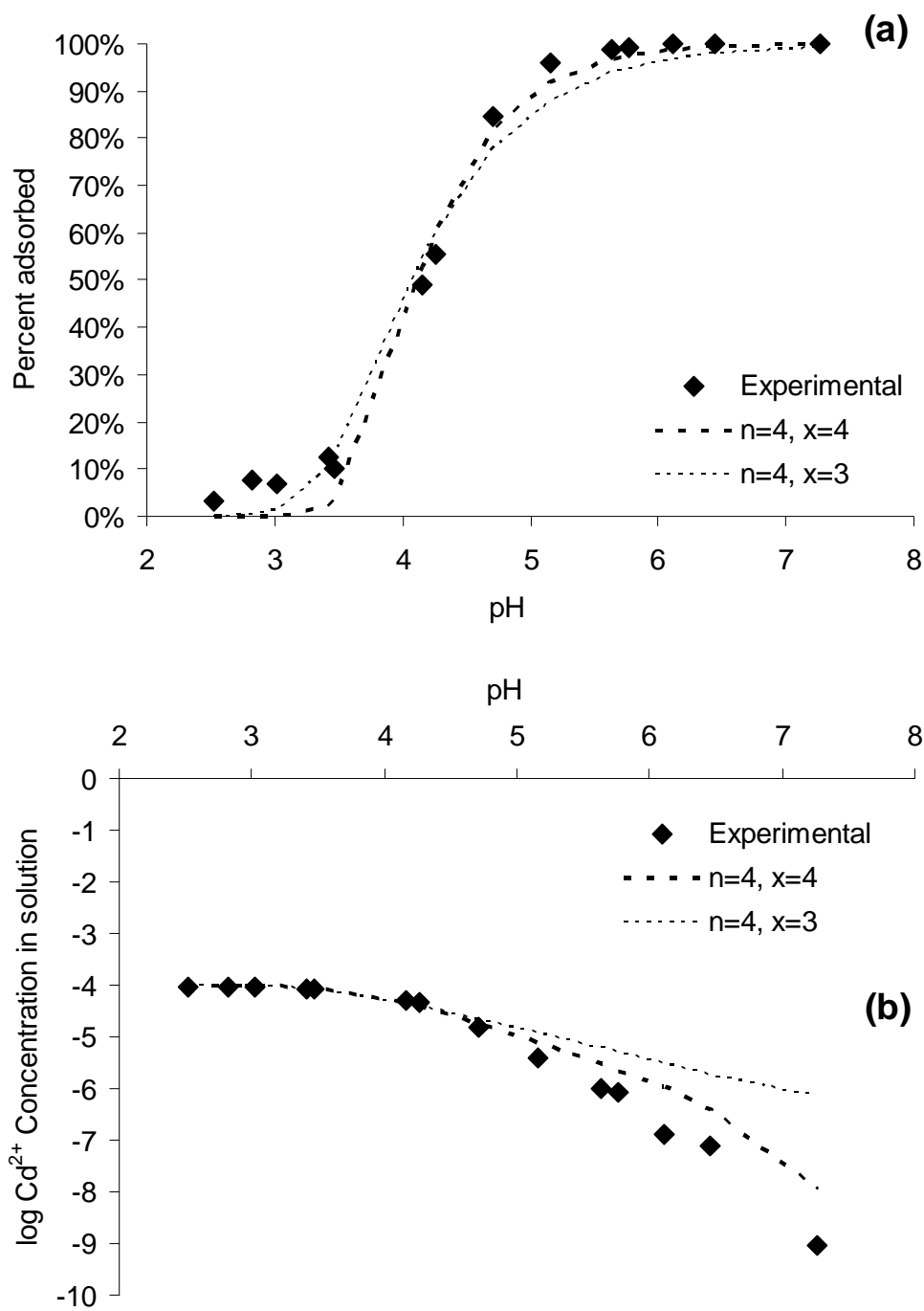


Figure 29. Multidentate model fits for Cd^{2+} on reduced PLC-RVC as percent adsorbed (a) and $\log \text{Cd}^{2+}$ concentration (b). Corresponding parameters are listed in Table 11.

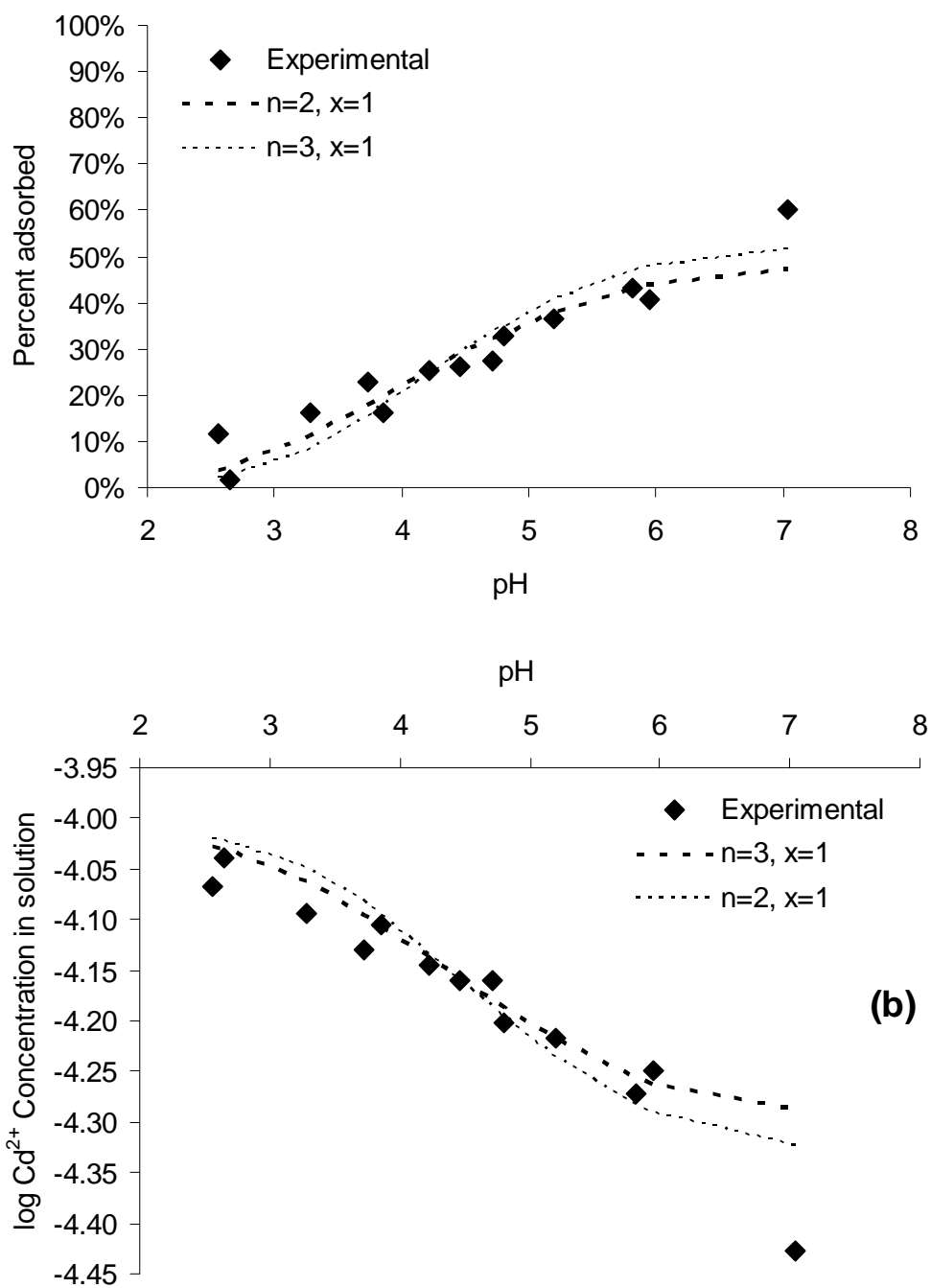


Figure 30. Multidentate model fits for Cd^{2+} on oxidized PLC-RVC RVC as percent adsorbed (a) and log Cd^{2+} concentration (b). Corresponding parameters are listed in Table 11.

The parameter sets with $n = 4$, $x = 4$ and $n = 4$, $x = 3$ had the lowest summed square absolute error in percent adsorption. Since both fits were very close in square error values, they were further evaluated by examining predictions of isotherm data for both fits as shown in Figure 29b. The set with $n = 4$, $x = 4$ fit the high end of the adsorption edge more closely than the $n = 4$, $x = 3$ set. Equilibrium data for isotherms were taken at the high end of the edge because that pH range is more characteristic of most wastes. Both sets underestimated adsorption at very low pH where there is no predicted adsorption. The underprediction at low pH has been observed in other surface complexation modeling efforts and may be the result of adsorption to a small set of high affinity sites [68].

For the oxidized edge the parameter sets that best fit the experimental data were $n = 3$, $x = 1$ and $n = 2$, $x = 2$. Both sets had similar square error, so both the percent adsorption and log metal concentration plots were examined. As in the case of the reduced edge, the high pH region of the edge was taken as the second criterion for deciding the best fit. In Figure 30a it is clear that both models flatten out in terms of percent adsorption below the data point near pH 7. Since there is only one point in this region its significance in the square error is diminished in relation to the other regions of the edge. Since the $n = 2$, $x = 1$ set more closely captures this point, and the total error between these two sets is comparable, the $n = 2$, $x = 1$ set was chosen as the best fit parameter set for the oxidized electrode.

The multidentate model has the ability to describe a wider range of pH behavior because of the inclusion of proton release. The multiple site interaction also affects the pH dependence since the key characteristic is not only the number of protons released but the stoichiometric ratio of protons released to sites consumed. It is possible that an additional adsorption contribution from carboxylate functional groups would improve the

model fits in both cases, but especially for the oxidized electrode for which the coordination number with oxygen increased. This additional complexity along with the addition of multiple sites and electrical interactions in the double layer could be pursued if more experimental data, specifically that with a varied ionic strength, were available.

4.5 NICKEL ADSORPTION RESULTS

The section presents results from nickel adsorption experiments and compares Ni^{2+} adsorption behavior to previously examined Cd^{2+} adsorption behavior. The selection of Ni as a second metal ion probe for evaluating adsorption in the ESIE system was due to its reduced binding constant to thiol groups compared to Cd^{2+} . In addition, binding constants for Ni^{2+} to the carboxylate group of amino acids such as glutamate are greater than reported values for Cd^{2+} .

4.5.1 pH dependent adsorption behavior of Ni^{2+}

Oxidized and reduced electrodes were exposed to solutions containing a total metal concentration of 6.3 mg/L and 22.8 mg/L for the reduced and oxidized electrodes, respectively. In both cases, the step-wise increases in the pH of the recirculating solution resulted in typical adsorption behavior for surface complexation of metal ions in which protons are released as the metal ion adsorbs as shown in Figure 31. This behavior was evident for both the oxidized and reduced PLC-RVC.

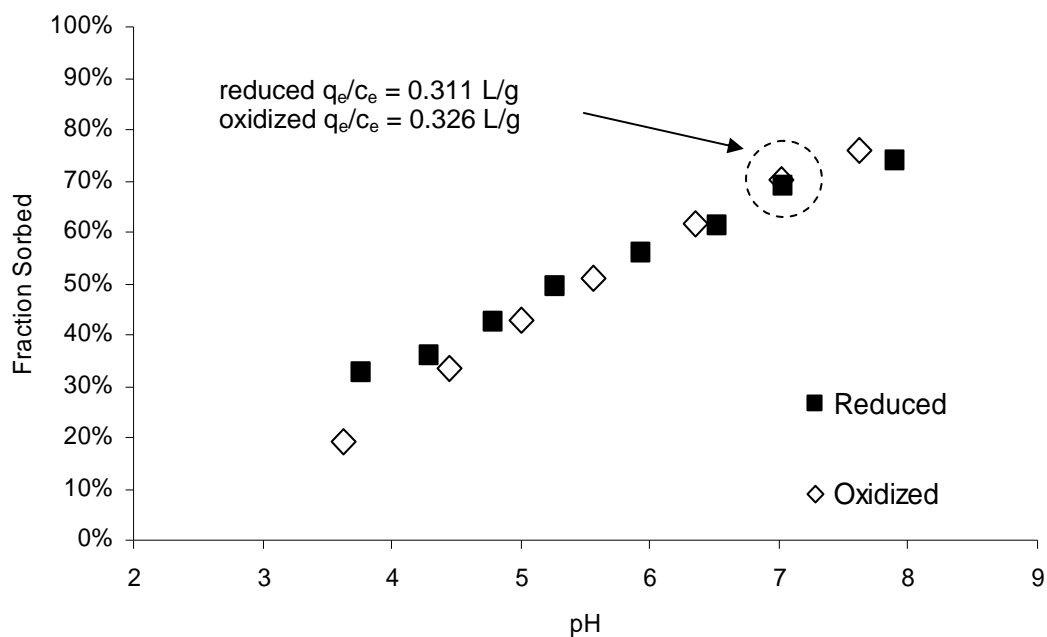


Figure 31. Ni^{2+} adsorption edge on DTT reduced and H_2O_2 oxidized PLC-RVC. The two conditions have different total metal concentrations of 6.3 mg/L for the reduced and 22.8 mg/L for the oxidized.

Both cases produced a change in adsorption over a wide range of pH in a manner similar to the Cd^{2+} oxidized electrode. As previously seen, this behavior is more typical of a weakly binding cation. The reduced state did not show a shift to stronger binding as in the case of Cd^{2+} . In fact, the Ni^{2+} binding is stronger on the oxidized electrode as the two edges have similar fraction adsorbed but the oxidized edge has a much higher total metal concentration. The ratio of metal adsorbed per gram solid (q_e) to metal in solution (c_e) was calculated for both conditions at the point circled in Figure 31 which was approximately pH 7. The oxidized edge has a slightly greater ratio (q_e/c_e) of 0.326 L/g compared to the reduced value of 0.311 L/g. Additionally the slope of the pH-adsorption transition decreased as a result of oxidation for Cd^{2+} , but for Ni^{2+} the slope of the oxidized edge is actually slightly steeper. These results imply that either there are more sites available on oxidized electrode, the coordination to the sites (and hence the binding

constant) is greater, or Ni^{2+} binds to different types of sites in the oxidized and reduced systems. However, broad edge, that encompasses a large pH range, indicates relatively weak binding in both cases.

4.5.2 Ni Adsorption Isotherm results

The result of stronger binding in the oxidized state is confirmed by the Ni^{2+} adsorption isotherms. The oxidized isotherm shows an increase in capacity for nickel. A possible explanation for this reversal in behavior between cadmium and nickel comes from the nature of ions and the functional groups on the PLC-RVC surface. Since Ni^{2+} is a hard metal acid it has a greater affinity for carboxylic acids than Cd^{2+} . For example, glutamic acid is an amino acid with a carboxylic acid functional group and forms complexes with Ni^{2+} . Stability constants for Ni^{2+} and Cd^{2+} with glutamate and cysteine are shown in Table 12.

Table 12. log K values for complexation of Ni and Cd with two representative amino acids

	Glutamate	Cysteine
NiL	6.5	10.7
NiL ₂	10.6	20.9
CdL	4.8	13
CdL ₂		19

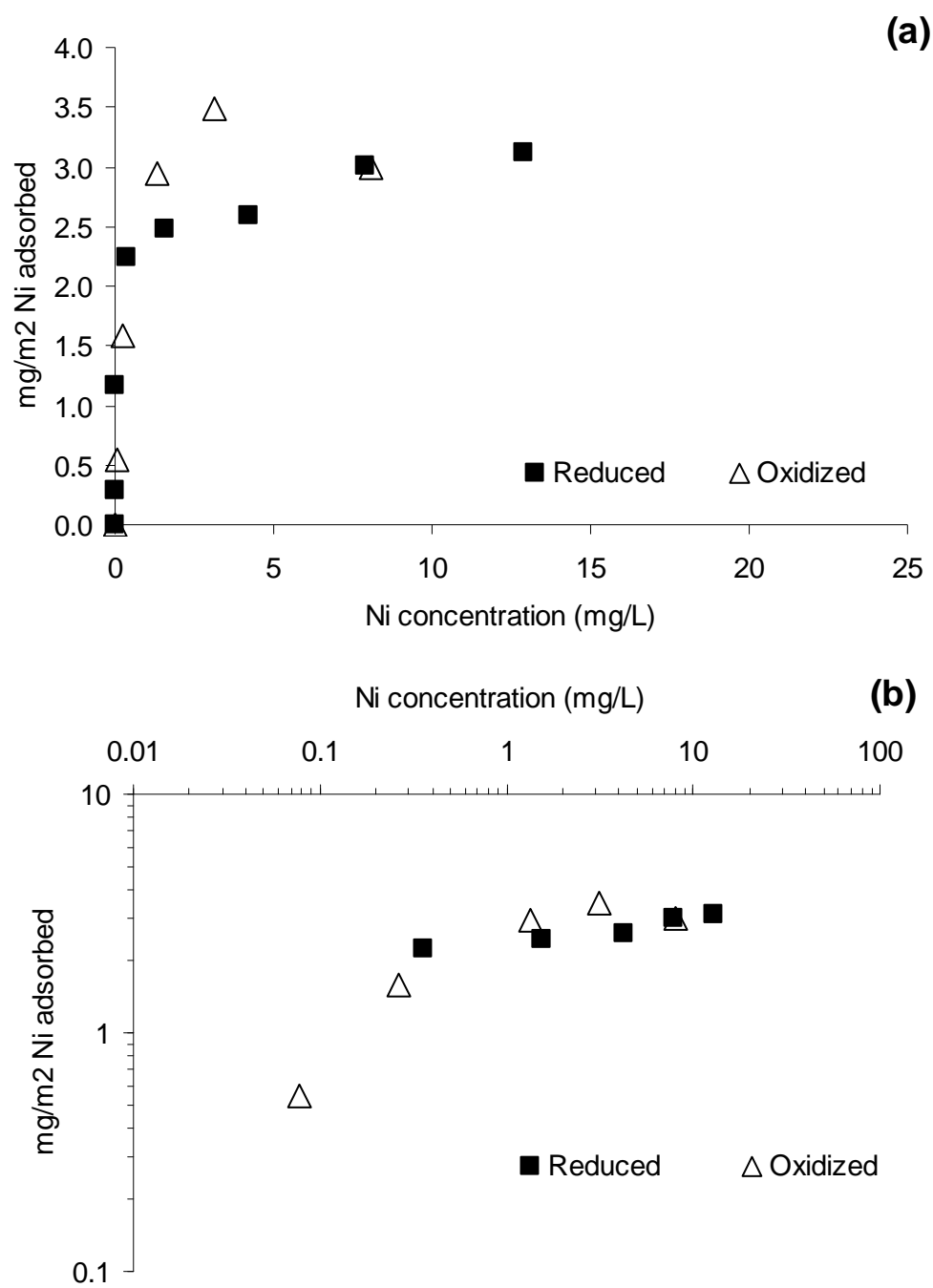


Figure 32. Ni²⁺ adsorption onto DTT reduced and H₂O₂ oxidized PLC-RVC electrodes. Normal scale (a) and log-log scale (b).

Carboxylic acids are present at the terminal end of the PLC molecule and also on the oxidized surface of the RVC electrode [69]. If the carboxylic acid concentration on the surface were high enough, it could drive Ni^{2+} adsorption even though Ni^{2+} has a significant complexation interaction with cysteine. Previous research with this same electrode by Strong et al., demonstrated that strong acid addition increased both the number of carboxylate groups and Ni^{2+} adsorption to the unmodified surface of the RVC electrode [69]. Cd^{2+} adsorption would not be affected as significantly because the difference between its carboxylate and thiol complexation constants span eight orders of magnitude, whereas the difference in nickel is only four orders of magnitude.

4.6 SUMMARY

Metal cation adsorption was examined on the ESIE apparatus to evaluate binding capacity and study the mechanisms of binding in the oxidized and reduced state. Batch equilibrium experiments showed approximately $3 \text{ mg/m}^2 \text{ Cd}^{2+}$ of reversible capacity between the reduced and oxidized states. Total capacity was found to be $10 \text{ mg/m}^2 \text{ Cd}^{2+}$ for reduced PLC-RVC and $6 \text{ mg/m}^2 \text{ Cd}^{2+}$ for oxidized. NaBH_4 irreversibly increased the capacity of the electrode by 3 mg/m^2 . Adsorption edge experiments showed a distinction between pH dependent adsorption on the oxidized and reduced surfaces. The reduced surface displays a typical pH dependence for strong binding cation metal adsorption with a transition from no binding to complete binding over 1-2 units of pH. The oxidized electrode adsorption edge had a much broader transition over 3-5 units of pH.

Analysis of XAS data for Cd^{2+} adsorption to the electrode further confirmed the distinction between the oxidized and reduced states of PLC-RVC by yielding a difference in coordination. Reduced PLC-RVC had sulfur and oxygen coordination numbers of 3.5 and 1.9, respectively. The oxidized state had decreased sulfur coordination and increased oxygen coordination of 2.2 and 2.8, respectively. The shift to greater sulfur coordination

in the presence of a higher concentration of thiols is confirmed by aqueous experiments found in the literature [66]. Bonding distances for Cd-S and Cd-O were similar for both the oxidized and reduced state in this work as well as in the study of aqueous complexation done by Frenkel et al. [66].

To explain the difference in pH behavior on adsorption, a pH dependent model was developed by extending a site limited model presented in Chapter 2. Proton release was incorporated into the adsorption reaction to form a baseline model. This model did not fully capture the effect of pH as it underestimated high pH adsorption for the reduced electrode and overestimated high pH adsorption for the oxidized electrode. The reduced experimental data had a steeper slope in the transition region and the reverse was true for the oxidized region. The model was further refined by allowing for multiple sites to interact with a single metal in a multidentate manner and multiple protons to be released. The rationale for multiple site interactions is derived from the XAS analysis and reinforced by literature observations of peptide metal interactions.

Ni²⁺ adsorption edge experiments showed a broad transition from no adsorption to maximum adsorption over 3-5 units of pH in a manner similar to the Cd oxidized edge. Nickel adsorption and edge experiments showed a redox trend opposite that of cadmium – more adsorption in the oxidized state. A possible explanation for this is the population of carboxylic acid groups on the PLC-RVC surface. If the concentration of these groups is high enough the carboxylate group could drive Ni²⁺ adsorption even though cysteine has a higher affinity for Ni²⁺.

Chapter 5: Conclusions and Recommendations

The ESIE system was developed and studied to improve upon existing metal removal technologies. Since metal contaminants cannot be degraded, the character and subsequent treatment of waste are important in the evaluation of the sustainability of a process. A modification to traditional ion exchange which employs a conductive resin and polypeptide functional group was considered for the purpose of reducing chemical regeneration requirements and subsequent waste generation. The ability to electrochemically change binding affinities allows metals to be released without having to completely overcome selectivity for contaminant ions. Several substrates were evaluated to provide a support material for the metal binding functional group while providing a conductive path for performing redox reactions on the functional group. Reticulated Vitreous Carbon (RVC) with poly-L-cysteine (PLC) functional groups provided a system selective for heavy metals and sensitive to redox chemistry.

Three primary hypothesis were tested on this system.

- I. Distinct oxidized and reduced states of the PLC-RVC electrode could be produced.
- II. The two oxidation states of the electrode have different metal ion adsorption properties.
- III. The oxidation states of the electrode can be switched by application of a potential.

Bulk adsorption data and spectroscopic data were used to test each of these hypotheses. First, it was shown that distinct oxidized and reduced states of the PLC-RVC electrode could be produced. Two metal ions, Cd(II) and Ni(II), with differing affinities for thiol and carboxylate ligands were used to probe the adsorption behavior of the

electrodes. The differences in adsorption behavior for each of these metal ions were used to compare differences in substrate character. Experiments showed that Ni^{2+} adsorption was enhanced by oxidation, whereas Cd^{2+} adsorption was enhanced by reduction. Reduction increases the number of free thiols which increases the adsorption of Cd^{2+} . Oxidation reduces the number of free thiols by converting them to disulfides and sulfonates, but also creates additional carboxylic acid functionality on the surface. The increase in carboxylate concentration will increase nickel binding. Cd^{2+} adsorption would not be affected as significantly because the difference between its carboxylate and thiol complexation constants span eight orders of magnitude, whereas the difference in nickel is only four orders of magnitude.

Second, the two oxidation states of the electrode were shown to have different metal ion adsorption properties. Cd^{2+} adsorption edge experiments showed distinct behavior for reduced and oxidized states. In the reduced state, adsorption showed a sharp transition from little binding to complete binding over 1-2 units of pH. On the other hand, the oxidized electrode showed a much broader transition region over 3-5 units of pH. In addition to different pH behavior, the reduced electrode had greater Cd^{2+} binding capacity than the oxidized electrode. Isotherm experiments run with reduction followed by oxidation decreased the total Cd^{2+} capacity by 0.3 mg over the surface of the electrode. The difference in adsorption behavior was independently verified by X-ray Absorption Spectroscopy (XAS) experiments. The reduced electrode showed greater coordination by sulfur ($N = 3.5$) than the oxidized electrode ($N = 2.2$). As sulfur coordination decreased, oxygen coordination increased from $N = 2.9$ to 1.8. Bonding distances were found to be similar in both conditions, which indicates that the nature of the Cd-S atomic interaction is similar in both cases. The difference in binding can be explained by a greater quantity of Cd-S interactions for each Cd atom.

Application of a multi-dentate model for Cd^{2+} adsorption was consistent with this explanation. A Langmuir site limited adsorption model was first modified by the addition of proton release with metal binding. This model could not fully describe both the sharp change in metal adsorption pH behavior on the reduced electrode and the shallow change in metal adsorption pH behavior on the oxidized electrode. The model was further refined with the addition of multi-dentate complexes (n) and multiple protons released on metal binding (x) based on the coordination information from EXAFS analysis. For the reduced Cd^{2+} adsorption edge, the parameter set $n = 4$, $x = 4$, $K = 0.021$ best fit the experimental data. For the oxidized Cd^{2+} adsorption edge, the parameter set $n = 2$, $x = 1$, $K = 5600 \text{ M}^{-1}$ best fit the experimental data. These parameters were in general agreement with the values obtained from EXAFS coordination.

Third, the oxidation states of the electrode can be switched by application of a potential. Comparison of reduced and oxidized adsorption isotherms that were conducted sequentially showed the ability to reduce and oxidize the PLC-RVC electrode with a variety of redox agents. A DTT treated reduced electrode was oxidized with H_2O_2 and Cd^{2+} capacity decreased. Subsequent reduction by electrochemical potential restored the lost capacity to that of the DTT electrode. A similar series of experiments was run with an NaBH_4 modified electrode. The modified electrode was electrochemically oxidized and capacity was decreased by the same quantity (0.3 g Cd) as the unmodified electrode. Chemical redox by DTT and H_2O_2 was equivalent to application of -0.8 and +0.8 V vs Ag/AgCl potentials in the ESIE system, respectively.

5.1 ENGINEERING IMPLICATIONS

The total capacity of the ESIE electrode for cadmium was 10 mg/m^2 relative to a 0.1 M HNO_3 rinsed electrode. On a mass basis this is 1.39 mg/g electrode or 0.012 mmol/g electrode. The redox reversible capacity of the electrode was 3 mg/m^2 of Cd^{2+}

(0.42 mg/g or 3.7 $\mu\text{mol/g}$). Previous work with PLC on controlled pore glass reached capacities of 20 $\mu\text{mol/g}$ [4] and 4.8 $\mu\text{mol/g}$ [3]. While ESIE represents an increase in total capacity over previous work, the process still falls an order of magnitude below the range of existing ion exchange resins (0.1 to 10 mmol/g) [9].

The reduced specific capacity requires a larger treatment unit to process a similar volume of water. The general design of the ESIE system is scalable, though one of the primary limitations is ensuring that the electrochemical processes are complete while minimizing current required. The size of the electrode can be increased until the voltage drop across the electrode or the voltage drop across the solution becomes significant relative to the total voltage applied. The geometry of the system and properties of the materials dictate the resistance of each component, and therefore the voltage drop. In addition to electrode size and geometry, electrolyte concentration is a significant design parameter in the overall performance of the system. Though the electrolyte concentration and its corresponding ionic strength are not true sizing parameters, it provides another variable which can be modified to adjust the performance of the ESIE system. The complexity of the electrochemical aspects of the process requires a systematic optimization between these parameters and current usage for large scale systems.

This increase in capital cost could be offset by the decrease in regeneration costs. The ESIE process used 0.05 M ionic strength solutions to perform oxidation and reduction to regenerate the resin. Typical ion exchange uses 1 to 2 M solutions for regeneration, which is 20 to 40 times greater in ionic strength [8]. ESIE regeneration solutions would be much easier and cheaper to treat as proposed at the outset of this work. The reduction in ionic strength can be seen as a tradeoff for the decreased capacity and immediately makes ESIE more competitive with traditional ion exchange.

5.2 RECOMMENDATIONS

The system has potential for improvement in performance and capacity and several characteristics remain to be studied. Increases in capacity can be made by lengthening the PLC peptide as seen in other peptide-metal binding designs [33]. Additionally an increase in specific surface area of the RVC electrode would increase capacity. The efficiency of the peptide attachment reaction directly affects the surface density of the peptide. In addition, areas of the electrode which are not accessible to long PLC molecules could be reached by subsequent attachment of cysteine to increase total surface coverage. The effect of competing ions such as sodium at high concentrations has yet to be established and plays an important role with respect to the ability of the ESIE system or any ion exchange system to operate under a variety of conditions.

Several electrochemical parameters of the system need further study in order to develop a method for optimizing a scaled up version of the process. The current consumed by the electrochemical process is split among the reaction of PLC, the charging of the double layer at the surface of the electrode, the resistance through the electrode material, and resistance in solution. Understanding the relative contribution of each of these current sinks is essential to any optimization of the ESIE system.

It is clear that the ESIE system is applicable to the remediation of heavy metal contaminated waters, but further work is necessary to establish the scenarios for which the system is economical in comparison to traditional ion exchange. Further development in ionic strength behavior, competition with other metals and electrochemical behavior will establish the robustness of the process.

Appendix – Model Calculations

The following description applies for both the baseline model and the multidentate model. The multidentate model reduces to the baseline model when $n = 1$ and $x = 1$.

To calculate the percent adsorption predicted by the model, Eqn. 4.8 and Eqns. 4.10-4.12 must be solved simultaneously. Since there is no analytical solution for arbitrary values of n and x , the equations must be solved numerically. The equations were rearranged in terms of metal concentration. To solve the system of equations, S_{TOT} , n , x , and K_a must be specified. For each pH where there is a data point a non-linear solver was used to find a value for $[Me^{2+}]$ such that:

$$S_{TOT} = n(Me^{2+}_{TOT} - [Me^{2+}]) + n \sqrt{\frac{(Me^{2+}_{TOT} - [Me^{2+}])[H^+]^x}{K[Me^{2+}]}} \left(1 + \frac{K_a}{[H^+]}\right) \quad \text{Eqn. A.1}$$

$[Me^{2+}]$ was then converted to percent adsorbed by Eqn 4.6. The series of model percent adsorbed values was then compared to the experimental percent adsorbed values at each data point. The absolute square of the difference between the percent adsorbed was summed over all data points to give an evaluation of the fit for that given set of parameters. The absolute difference in percent adsorbed was chosen as it weights the points in the transition area of the edge the most.

Glossary

ESIE - Electronically Switchable Ion Exchange

PLC - poly-L-cysteine

RVC - Reticulated Vitreous Carbon

CV - Cyclic Voltammetry

MALDI-TOF - Matrix Assisted Laser Desorption/Ionization - Time of Flight

XAS - X-Ray Absorption Spectroscopy

XANES - X-Ray Absorption Near Edge Structure

EXAFS - Extended X-Ray Absorption Fine Structure

DTT - dithiothreitol

SHE - Standard Hydrogen Electrode

References

1. Vernet, J.P., *Impact of heavy metals on the environment*. 1992, Amsterdam; New York: Elsevier.
2. Harrison, P.M.a.E., *Topics in Molecular and Structural Biology, Vol 6: Metalloproteins, Pt. 1: Metal Proteins with Redox Roles*. Vol. 6. 1985. 149-181.
3. Howard, M., H.A. Jurbergs, and J.A. Holcombe, *Effects of Oxidation of Immobilized Poly(L-Cysteine) on Trace Metal Chelation and Preconcentration*. Analytical Chemistry, 1998. **70**(8): p. 1604-1609.
4. Jurbergs, H.A. and J.A. Holcombe, *Characterization of Immobilized Poly(L-cysteine) for Cadmium Chelation and Preconcentration*. Analytical Chemistry, 1997. **69**(10): p. 1893-1898.
5. Miller, T.C., et al., *An in Situ Study of Metal Complexation by an Immobilized Synthetic Biopolymer Using Tapping Mode Liquid Cell Atomic Force Microscopy*. Analytical Chemistry, 2001. **73**(17): p. 4087-4095.
6. Johnson, A. and J.A. Holcombe, *Poly(L-cysteine) as an electrochemically modifiable ligand for trace metal chelation*. Analytical Chemistry, 2005(77): p. 30-35.
7. *National Primary Drinking Water Regulations*. 2009 [cited; Available from: <http://www.epa.gov/safewater/consumer/pdf/mcl.pdf>].
8. *Control and Treatment Technology for the Metal Finishing Industry - Ion Exchange*. 1981, Environmental Protection Agency.
9. Tchobanoglous, G., F.L. Burton, and H.D. Stensel, eds. *Wastewater Engineering, Treatment and Reuse*. 2003, McGraw Hill: New York. 1819.
10. Rodriguez, J., et al., *Feasibility assessment of electrocoagulation towards a new sustainable wastewater treatment*. Environmental Science and Pollution Research International, 2007. **14**(7): p. 477-482.
11. Haggerty, G.M. and R.S. Bowman, *Sorption of chromate and other inorganic anions by organo-zeolite*. Environmental Science and Technology, 1994. **28**(3): p. 452-8.
12. Bridger, N.J., C.P. Jones, and M.D. Neville, *Electrochemical Ion Exchange*. Journal of Chem. Tech. Biotechnol., 1991. **50**: p. 469-481.
13. Harnisch, J.A. and M.D. Porter, *Electrochemically modulated liquid chromatography: an electrochemical strategy for manipulating chromatographic retention*. Analyst, 2001. **126**(11): p. 1841-1849.
14. Harnisch, J.A., et al., *Chemical modification of carbonaceous stationary phases by the reduction of diazonium salts*. Analytical chemistry, 2001. **73**(16): p. 3954-9.
15. Ponton, L., M. and M. Porter, D., *Electrochemically modulated liquid chromatographic separations of inorganic anions*. Journal of chromatography, 2004. **1059**(1-2): p. 103-9.
16. Ge, H., P.R. Teasdale, and G.G. Wallace, *Electrochemical chromatography - packings, hardware and mechanisms of interaction*. Journal of Chromatography, 1991. **544**(1-2): p. 305-16.

17. Lilga, M.A., et al., *Metal ion separations using electrically switched ion exchange*. Separation and Purification Technology, 1997. **11**(3): p. 147-158.
18. Rassat, S.D., et al., *Development of an electrically switched ion exchange process for selective ion separations*. Separation and Purification Technology, 1999. **15**(3): p. 207-222.
19. Oklejas, V., et al., *Electric-Field Control of the Tautomerization and Metal Ion Binding Reactivity of 8-Hydroxyquinoline Immobilized to an Electrode Surface*. Analytical Chemistry, 2008. **80**(6): p. 1891-1901.
20. Shriver, D.F., P.W. Atkins, and C.H. Langford, *Inorganic Chemistry*. 1996. 740.
21. Elmahadi, H.A.M. and G.M. Greenway, *Immobilized alga as a reagent for preconcentration in trace element atomic absorption spectrometry*. Journal of Analytical Atomic Spectrometry, 1991. **6**(8): p. 643-6.
22. Ghosh, M. and S.P. Singh, *Effect of cadmium and lead on growth of Ipomea cranea - a phytoremediation study*. Pollution Research, 2003. **22**(4): p. 561-568.
23. Liu, X.-b. and B.-s. Xing, *Phytoextraction: a cost-effective approach to metal-contaminated soils*. Journal of Northeast Agricultural University (English Edition), 2003. **10**(2): p. 182-187.
24. Kadish, K.M., et al., *The Porphyrin Handbook: Volume 17 / Phthalocyanines: Properties and Materials*. 2003. 289 pp.
25. Malachowski, L., J.L. Stair, and J.A. Holcombe, *Immobilized peptides/amino acids on solid supports for metal remediation*. Pure and Applied Chemistry, 2004. **76**(4): p. 777-787.
26. Stillman, M.J., et al., *Metallothioneins: Synthesis, Structure and Properties of Metallothioneins, Phytochelatins and Metal-Thiolate Complexes*. 1992. 443.
27. Maret, W., *Oxidative metal release from metallothionein via zinc-thiol/disulfide interchange*. Proceedings of the National Academy of Sciences of the United States of America, 1994. **91**(1): p. 237-41.
28. Anderson, B.R., *Evaluation of immobilized metallothionein for trace metal separation and preconcentration*, in *Chemistry*. 1994, The University of Texas at Austin: Austin, TX. p. 215.
29. Veglia, G., et al., *The Structure of the Metal-Binding Motif GMTCAAC Is Similar in an 18-Residue Linear Peptide and the Mercury Binding Protein MerP*. Journal of the American Chemical Society, 2000. **122**(10): p. 2389-2390.
30. Pantoliano, M.W., et al., *The engineering of binding affinity at metal ion binding sites for the stabilization of proteins: subtilisin as a test case*. Biochemistry, 1988. **27**(22): p. 8311-17.
31. Arnold, F.H. and B.L. Haymore, *Engineered metal-binding proteins: purification to protein folding*. Science, 1991. **252**(5014): p. 1796-7.
32. Gutierrez, E., et al., *Characterization of Immobilized Poly-L-aspartate as a Metal Chelator*. Environmental Science and Technology, 1999. **33**(10): p. 1664.
33. Stair, J., L. and J. Holcombe, A., *Metal binding characterization and conformational studies using Raman microscopy of resin-bound poly(aspartic acid)*. Analytical chemistry, 2007. **79**(5): p. 1999-2006.

34. Malachowski, L. and J.A. Holcombe, *Comparison of immobilized poly-L-aspartic acid and poly-L-glutamic acid for chelation of metal cations*. *Analytica Chimica Acta*, 2004. **517**(1-2): p. 187-193.
35. Stair, J., L., et al., *Quantitative determination of single-bead metal content from a peptide combinatorial library*. *Journal of combinatorial chemistry*, 2006. **8**(6): p. 929-34.
36. Malachowski, L. and J.A. Holcombe, *Immobilized poly-L-histidine for chelation of metal cations and metal oxyanions*. *Analytica Chimica Acta*, 2003. **495**(1-2): p. 151-163.
37. Miller, T.C. and J.A. Holcombe, *Characterization of metal ion-exchange on modified surfaces of porous carbon*. *Analytica Chimica Acta*, 2002. **455**(2): p. 233-244.
38. Autry, H. and J.A. Holcombe, *Cadmium, copper and zinc complexes of poly-L-cysteine*. *Analyst*, 1995. **120**(10): p. 2643-7.
39. White, B.R., B.T. Stackhouse, and J.A. Holcombe, *Magnetic gamma-Fe₂O₃ nanoparticles coated with poly-L-cysteine for chelation of As(III), Cu(II), Cd(II), Ni(II), Pb(II) and Zn(II)*. *Journal of Hazardous Materials*, 2009. **161**(2-3): p. 848-853.
40. White, B.R., H.M. Liljestrand, and J.A. Holcombe, *A 'turn-on' FRET peptide sensor based on the mercury binding protein MerP*. *Analyst*, 2008. **133**(1): p. 65-70.
41. Chow, E. and J.J. Gooding, *Peptide modified electrodes as electrochemical metal ion sensors*. *Electroanalysis*, 2006. **18**(15): p. 1437-1448.
42. Beguin, F. and E. Frackowiak, eds. *Carbon Materials for Electrochemical Energy Storage Systems*. 2010, CRC Press: Boca Raton, FL. 529.
43. ERGAerospace. *ERG: What is Duocel & How is it Specified? - Duocel Foam Properties*. 2008 [cited 2008 October 20th]; Available from: <http://www.ergaerospace.com/foamproperties/introduction.htm>.
44. Wang, J., *Reticulated vitreous carbon. A new versatile electrode material*. *Electrochimica Acta*, 1981. **26**(12): p. 1721-6.
45. ERGAerospace. *ERG: Introduction to Carbon Foam- Duocel*. 2009 [cited 2009 12/02/2009]; Available from: http://www.ergaerospace.com/carbon_foam.htm.
46. Bard, A.J. and L.R. Faulker, *Electrochemical Methods: Fundamentals and Applications*. 2001, New York: John Wiley and Sons, Inc.
47. Brown, W.D., *Reduction of protein disulfide bonds by sodium borohydride*. *Biochimica et Biophysica Acta*, 1960. **44**: p. 365-7.
48. Brown, G.E., Jr., *Spectroscopic studies of chemisorption reaction mechanisms at oxide-water interfaces*. *Reviews in Mineralogy*, 1990. **23**(Miner.-Water Interface Geochem.): p. 309-63.
49. Webb, S., *SixPACK*. 2009, Stanford Synchrotron Radiation Laboratory: Menlo Park, CA.
50. George, G.N. and I.J. Pickering, *EXAFSPAK*. 1995, Stanford Synchrotron Radiation Laboratory: Menlo Park, CA.
51. Newville, M., *IFEFFIT*. 2009, Consortium for Advanced Radiation Sources: Chicago, IL.

52. Ankudinov, A.L., et al., *Real-space multiple-scattering calculation and interpretation of x-ray-absorption near-edge structure*. Physical Review B: Condensed Matter and Materials Physics, 1998. **58**(12): p. 7565-7576.
53. Brown, G.E., Jr., et al., *X-ray absorption spectroscopy and its applications in mineralogy and geochemistry*. Reviews in Mineralogy, 1988. **18**(Spectrosc. Methods Mineral. Geol.): p. 431-512.
54. Chen, J., S. Yiacoumi, and T.G. Blaydes, *Equilibrium and kinetic studies of copper adsorption by activated carbon*. Separations Technology, 1996. **6**(2): p. 133-146.
55. Papelis, C., P.V. Roberts, and J.O. Leckie, *Modeling the Rate of Cadmium and Selenite Adsorption on Micro- and Mesoporous Transition Aluminas*. Environmental Science and Technology, 1995. **29**(4): p. 1099-108.
56. *CRC Handbook of Chemistry and Physics*. 90th ed. 2009-2010: CRC Press.
57. Luo, D. and B.D. Anderson, *Application of a two-state kinetic model to the heterogeneous kinetics of reaction between cysteine and hydrogen peroxide in amorphous lyophiles*. Journal of Pharmaceutical Sciences, 2008. **97**(9): p. 3907-3926.
58. Ashby, M.T. and P. Nagy, *Revisiting a proposed kinetic model for the reaction of cysteine and hydrogen peroxide via cysteine sulfenic acid*. International Journal of Chemical Kinetics, 2006. **39**(1): p. 32-38.
59. Paquette, L.A., et al., *Encyclopedia of Reagents for Organic Synthesis*, L.A. Paquette, Editor. 2009, John Wiley & Sons, Inc.
60. Pickering, I.J., et al., *X-ray absorption spectroscopy of cadmium phytochelatin and model systems*. Biochimica et Biophysica Acta, 1999. **1429**(2): p. 351-364.
61. Jalilehvand, F., et al., *Cadmium(II) Cysteine Complexes in the Solid State: A Multispectroscopic Study*. Inorganic Chemistry, 2009. **48**(9): p. 4219-4230.
62. Malferrari, D., et al., *Sorption kinetics and chemical forms of Cd(II) sorbed by thiol-functionalized 2:1 clay minerals*. Journal of Hazardous Materials, 2007. **143**(1-2): p. 73-81.
63. Tarulli, S.H., et al., *Structural and spectroscopic characterization of bis(thiosaccharinato)bis(benzimidazole)cadmium(II)*. Journal of Molecular Structure, 2006. **797**(1-3): p. 56-60.
64. Karlsson, T., P. Persson, and U. Skyllberg, *Extended X-ray Absorption Fine Structure Spectroscopy Evidence for the Complexation of Cadmium by Reduced Sulfur Groups in Natural Organic Matter*. Environmental Science and Technology, 2005. **39**(9): p. 3048-3055.
65. Karlsson, T., et al., *Complexation of cadmium to sulfur and oxygen functional groups in an organic soil*. Geochimica et Cosmochimica Acta, 2007. **71**(3): p. 604-614.
66. Frenkel, A.I., A. Vairavamurthy, and M. Newville, *A study of the coordination environment in aqueous cadmium-thiol complexes by EXAFS spectroscopy: experimental vs theoretical standards*. Journal of Synchrotron Radiation, 2001. **8**(2): p. 669-671.
67. Stumm, W. and J.J. Morgan, *Aquatic Chemistry: Chemical Equilibria and Rates in Natural Waters; Third Edition*. 1995. 1022 pp.

68. Schaller, M.S., et al., *Surface complexation modeling of Cd(II) adsorption on mixtures of hydrous ferric oxide, quartz and kaolinite*. Journal of Colloid and Interface Science, 2009. **339**(2): p. 302-309.
69. Strong, W.R., et al., *Introduction of ion-exchange moieties to reticulated vitreous carbon by direct chemical modification*. Carbon, 2006. **44**(10): p. 1936-1941.

Vita

Ramakrishnan Kannappan was born to Sockalingam and Meenakshi Kannappan on December 13th, 1980 in Houston, Texas. After attending Clear Lake High School in Houston, he entered as a freshman at The University of Texas at Austin in the Fall of 1998. He earned a Bachelors degree in Chemical Engineering in the Fall of 2001 and continued on as a research assistant under C. Grant Willson. In the Fall of 2002 he joined the Environmental and Water Resources Engineering program at Texas and received a Masters degree in the Fall of 2004. Following his masters he continued at Texas pursuing his PhD under Lynn Katz with support from James Holcombe.

Permanent address: 11415 Sagemorgan Drive, Houston, TX 77089

This dissertation was typed by the author.